GEOLOGICA CARPATHICA, AUGUST 2020, 71, 4, 361–381 https://doi.org/10.31577/GeolCarp.71.4.5

The Late Cretaceous A-type alkali-feldspar granite from Mt. Požeška Gora (N Croatia): Potential marker of fast magma ascent in the Europe–Adria suture zone

DRAŽEN BALEN[1], PETRA SCHNEIDER[1,✉], HANS-JOACHIM MASSONNE[2], JOACHIM OPITZ[2], JARMILA LUPTÁKOVÁ[3], MARIÁN PUTIŠ[4] and ZORICA PETRINEC[1]

[1]Department of Geology, Faculty of Science, University of Zagreb, Horvatovac 95, 10000 Zagreb, Croatia; drbalen@geol.pmf.unizg.hr, ✉pschneider@geol.pmf.unizg.hr, zoricap@geol.pmf.unizg.hr
[2]Institut für Mineralogie und Kristallchemie (closed), Universität Stuttgart, Azenbergstraβe 18, 70174 Stuttgart, Germany; h-j.massonne@imi.uni-stuttgart.de, joachim.opitz@imi.uni-stuttgart.de
[3]Earth Science Institute, Slovak Academy of Sciences, Ďumbierska 1, 974 01 Banská Bystrica, Slovakia; luptakova@savbb.sk
[4]Department of Mineralogy and Petrology, Faculty of Natural Sciences, Comenius University, Ilkovičova 6, 84104 Karlova Ves, Bratislava, Slovakia; marian.putis@uniba.sk

(Manuscript received February 12, 2020; accepted in revised form June 22, 2020; Associate Editor: Igor Broska)

Abstract: An alkali-feldspar granite (Požega granite) of reddish colour occurs in northern Croatia in the Cretaceous suture zone (Sava Zone) between the collided plates of Europe and Adria (Africa). This granite is mainly composed of alkali feldspar (perthite) and quartz, with small amounts of albite. Accessories are hematite with ilmenite exsolution, zircon, apatite and monazite. Anatase, rutile (?), kokchetavite, and kumdykolite are found only as inclusions in zircon. The granite shows a geochemical signature typical for an A_2-subtype granite, characterized by a peraluminous, highly siliceous and alkaline composition, and belongs to the group of oxidized and ferroan granites with low CaO, MgO, and MnO contents and high FeO_T/FeO_T+MgO ratios. Trace element contents plotted in chondrite and primitive mantle normalized element diagrams show positive anomalies of K, Pb, and Zr and negative anomalies of Ba, Nb, P, Eu, and Ti. Based on whole-rock geochemical data, the magma originated mainly from melting of lower continental crust. According to the zircon typology (D and J5 types prevail), zircon and whole-rock chemistry, and high Zr-saturation temperatures (T=860–950 °C), the melting process at high temperature and dry conditions could have been triggered by upwelling hot mantle. The ascent of the thus produced A-type granitic magma into the Europe–Adria suture was fast. The Požega granite indicates the transition from compression to extension accompanied by opening of a sedimentary basin. According to the $^{206}Pb/^{238}U$ versus $^{207}Pb/^{235}U$ concordia age determined on zircon, this event occurred 83.6±1.5 Ma ago.

Keywords: A-type granite, zircon, Sava Zone, Europe–Adria collision, Cretaceous.

Introduction

The closure of the western branch of the Neotethys Ocean took place through convergence of the Adria microplate toward Europe. This convergence formed a suture zone named the Sava Zone (e.g., Pamić 1993; Schmid et al. 2008). This zone is a complex geotectonic unit which represents a suture between the Dinarides (as a part of the Adria microplate) and the Tisia (Tisza) tectonic Mega-Unit (as a part of Europe). It is composed of an ophiolite (the remnants of the former Sava Back-Arc Basin, in literature also termed the Sava Back-Arc Ocean or Sava Ocean), with related magmatic, sedimentary and metamorphic rocks (e.g., Pamić 1993, 2002; Pamić et al. 2002a,b; Schmid et al. 2008, 2020; Ustaszewski et al. 2009, 2010; Handy et al. 2015). The Sava Zone extends from Zagreb toward the south-east of Belgrade, and further to the south through the Vardar Zone into southern Serbia, North Macedonia and Greece (Fig. 1; Schmid et al. 2008; Ustaszewski et al. 2010). The north-western end of the Sava Zone close to Zagreb sharply turns into the SW–NE strike of the Mid-Hungarian fault zone and is further buried below the Cenozoic cover of the Pannonian Basin (Schmid et al. 2020). The formation of the Sava Zone took place from the Late Cretaceous to the Early Paleogene until the final collision of the Dinarides with the Tisia Mega-Unit (Pamić 2002).

Exposures of the late Mesozoic and Cenozoic igneous rocks of the Sava Zone occur in northern Bosnia (Mts. Kozara, Prosara and Motajica), northern Serbia (Mt. Fruška Gora) and eastern Croatia (Mts. Požeška Gora and Moslavačka Gora) (Schmid et al. 2008). The rocks are related to the magmatism along the Europe–Adria suture zone. Unfortunately, these rocks are relatively rare and therefore investigated in detail lately, especially from the point of view of accessory minerals and their geochemistry. Zircon stands out as a particularly significant accessory mineral of igneous rocks (e.g., Hoskin & Schaltegger 2003) with the potential to resolve age and petrogenetic issues of the Europe–Adria suture zone.

The Upper Cretaceous alkali-feldspar granite, which occurs in northern Croatia near the town of Požega (Fig. 1), bears the geochemical signature of an A-type granite (Pamić 1987;

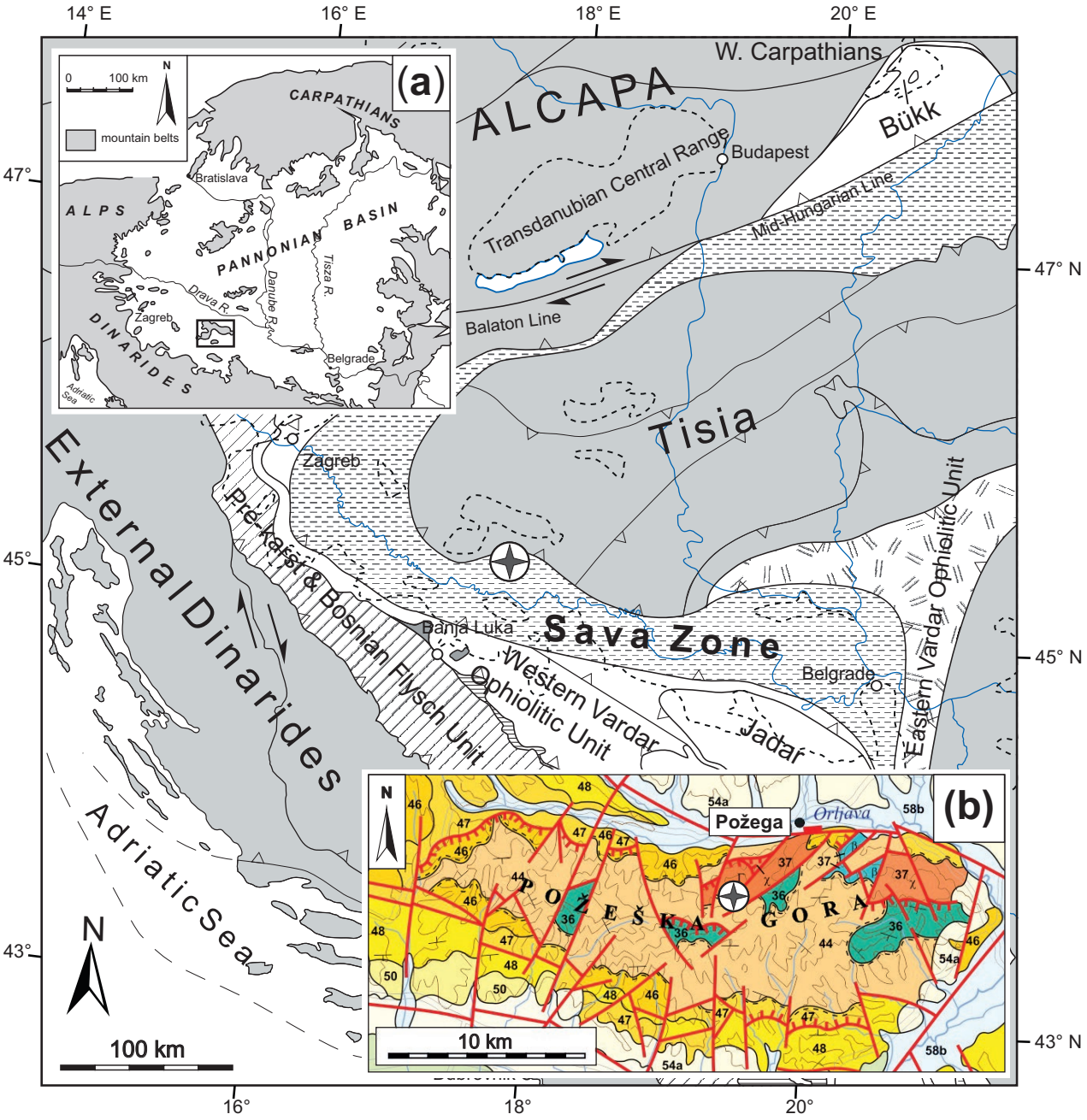

Fig. 1. Simplified map of the Dinaride–Alpine–Pannonian region showing the major structural units after Schmid et al. 2008 (map is slightly modified after Lužar-Oberiter et al. 2012) with insets that show the position of **(a)** the main mountain belts and Pannonian Basin and **(b)** a Mt. Požeška Gora geological map (after Šparica et al. 1979, 1980; Pamić 1987; Croatian Geological Survey 2009). The position of the study area is marked by the rectangle and circled stars. Legend: 58b — alluvial deposits (Holocene); 54a — loess (Pleistocene); 50 — "Paludina beds" (Pliocene); 48 — clastic rocks and coal (Miocene, M_7); 47 — carbonate clastic deposits (Miocene, $M_{5,6}$); 46 — "litavac" (bioclastic beech carbonate) and clastites with volcanic rocks (Miocene, M_4); 44 — clastites and carbonates (Miocene, $M_{2,3}$); 37 — igneous rocks (Late Cretaceous, Paleogene): β — basalts, χ — rhyolites, Γ — granites; 36 — carbonate clastic deposits (flysch) and Scaglia limestones (Late Cretaceous).

Pamić & Lanphere 1991; Pamić et al. 2000). The occurrence of this rather small body is of particular importance as this type of granite usually marks the beginning of extensional processes (e.g., Eby 2011; Grebennikov 2014). Consequently, the occurrence of an A-type granite, located within the Late Cretaceous collision zone that marks the Europe–Adria plate boundary zone, may be a marker of the change from collision to extension.

The Upper Cretaceous (Maastrichtian) age of 71.5±2.8 Ma was determined using the Rb–Sr isochron method on granite and rhyolite samples with the assumption of a co-genetic relation between them (Pamić et al. 1988). However, the finding

of red granite pebbles and fragments at the base of the Santonian–Campanian–Maastrichtian stratigraphic section (Šparica et al. 1979, 1980; Jamičić 2007) is in contradiction with the reported dating. Since the position of this peculiar granite has further geodynamic implications for the evolution of the Sava Zone, a more precise determination of the granite age is important. In addition, the more detailed granite geochemistry to confirm the already postulated A-type signature, as well as that of accessory minerals and their characteristics, may shed light on the details of magmatism in the Croatian segment of the Late Cretaceous suture zone between Europe and Adria.

In this paper, we present petrographic and geochemical characteristics (major and trace including rare-earth elements =REE) of the Požega granite, together with U–Th–Pb zircon dating and zircon geochemistry in an attempt to unravel and constrain the origin of the granitic magma, the evolution of this granite and its significance for the geodynamics of the Europe–Adria collision.

Geological setting

Within the Sava Zone only a few exposures of various types of Cretaceous granitic rocks can be found (e.g., Mt. Moslavačka Gora, Mt. Prosara and Mt. Kozara), with the distinctive Požega granite described in this paper being among them. Mt. Požeška Gora represents a small exposed part of the border area (Fig. 1) between the Tisia (Tisza) tectonic Mega-Unit and the Dinarides, which belong to the European and Adria plates, respectively. The Požega granite is spatially associated with basalts and rhyolites that are members of an Upper Cretaceous volcanic-sedimentary complex (Šparica et al. 1979, 1980). The granite crops out at only a few places. Both the volcanic-sedimentary complex and the granite (Fig. 1) are covered mostly with Quaternary and Neogene sediments. Conglomerates, sandstones, breccias, laminated siltstones, and limestones, partially thick-bedded, comprise the sedimentary part of the complex, whereas basalt, albite rhyolite, and alkali-feldspar granite represent the magmatic part of the complex of Mt. Požeška Gora (Belak et al. 1998). The volcanic association covers an area of about 30 km^2 whereas the granite occurs, hidden under soil and vegetation, over a total area of approx. 6–7 km^2 (Pamić 1987). Fresh samples of granite are reduced to a single quarry. The granite is in tectonic and/or erosional–tectonic contact with Upper Cretaceous sediments and volcanic rocks (Šparica et al. 1979, 1980; Pamić 1987; Belak et al. 1998).

It should be noted that, beside Cretaceous volcanic rocks, similar Neogene volcanic rocks are also present in the area (Croatian Geological Survey 2009; Šparica et al. 1979, 1980). To avoid confusion we focused our research on the intrusive rocks (granite) only.

Is has been argued that the melts that produced the (tholeiitic) basaltic rocks of the volcanic-sedimentary complex were generated in the upper mantle and emplaced in an extensional zone within the continental crust (Pamić et al. 1988/89; Belak et al. 1998). According to Pamić et al. (1988, 1988/89), rhyolite and granite are co-genetic and originated from partial melting of continental crust within a magmatic arc of the northernmost Dinarides (Pamić 1987).

Analytical methods

Mineral analytics

Chemical analyses, back-scattered electron (BSE) images, cathodoluminescence (CL) images, and X-ray compositional maps for minerals and mineral assemblages were obtained with a CAMECA SX100 electron probe micro-analyser (EPMA). The qualitative identification of the mineral phases was achieved by means of energy-dispersive X-ray spectrometry (EDS). For full quantitative analysis wavelength-dispersive X-ray spectrometry (WDS) was used. Operational conditions (except for zircon) included an acceleration voltage of 15 kV, a beam current of 15 nA, and a beam diameter of about 3 μm with 20 seconds counting time on both peak and background of each selected X-ray radiation line. Reference materials were natural minerals and pure oxides (albite, periclase, corundum, wollastonite, orthoclase, rutile, rhodonite, fayalite, barite, Cr_2O_3); Kα lines were used except the Lα line for Ba. The PAP correction procedure provided by CAMECA was utilized. The structural formulae for hematite and feldspar were calculated on the basis of 3 O and 8 O, respectively (Table 1).

For the internal calibration of LA-ICP-MS measurements, elemental contents in zircon measured in thin sections with the EPMA and J43_Zir, Hf, $LaPO_4$, $CePO_4$, YPO_4, and UO_2-Cann reference materials were used. The EPMA analyses of zircon were undertaken with an acceleration voltage of 15 kV, a beam current of 20 nA, and 20 seconds counting times on the peak and 10 seconds (20 s for Zr) on the background. The obtained reference value averaging 12 analyses is Zr=49.059 wt. %.

Whole-rock chemistry

The samples (ca. 2–2.5 kg in weight) were collected during multiple field campaigns and assessed for alteration using thin sections. These samples were crushed in a jaw crusher, powdered in an agate mill, and analyzed at the Bureau Veritas Commodities Canada Ltd (Vancouver) by inductively coupled plasma mass spectrometry (ICP-MS; trace elements including REE) and inductively coupled plasma emission spectrometry (ICP-ES; major elements). Powders were air-dried and sieved through a 0.125 mm stainless-steel screen. The sample preparation included the splitting of 0.2 g rock powder each for $LiBO_2/Li_2B_4O_7$ fusion for ICP-ES and for ICP-MS. Natural rocks of known composition and pure quartz were used as reference materials. The analytical accuracy was controlled using internal geological reference materials, the compositions of which are comparable to the rocks in this study (STD

GS311-1, STD GS910-4, STD DS10, STD OREAS45EA, STD SO-19). Detection limits are shown in Table 2. Reference materials were certified in-house by analysis with CANMET Certified Reference Materials. Loss on ignition (LOI) was determined by weight difference before and after 4 hours ignition at 1000 °C. Geochemical data and diagrams are recalculated and handled with the GCDkit software (Janoušek et al. 2006).

Raman spectroscopy

Separated zircon grains were analyzed using micro-Raman spectroscopy in order to determine the type of inclusions in zircon. Analyses were performed with a Horiba Jobin-Yvon LabRam HR 800 spectrometer equipped with a Czerny-Turner monochromator, 600 grooves per mm grating, a Peltier-cooled charge-coupled device (CCD) detector, and coupled to an Olympus BX41 microscope with a long working distance 100×/0.8 objective. Zircon crystals were irradiated by a He–Ne (633 nm) laser with a power of about 3 mW on the sample. A Nd:YAG (532 nm) laser was used only for verifying possible luminescence effects. The Rayleigh line (0 cm^{-1}) and emission bands of Ne glow lamps were used for calibration. Wavenumber accuracy is better than 0.8 cm^{-1}. Lateral resolution of the system was better than 1 μm, and the spectral resolution was ~3.6 cm^{-1} (red spectral range). The spectra of the unknown phases were collected in the range of 70–4000 cm^{-1} to cover also the region of OH-stretching bands. Obtained spectra were compared with available databases and literature (e.g., Kanzaki et al. 2012; Kotková et al. 2014; Hurai el al. 2015; Ferrero et al. 2016).

Scanning electron microscopy

Scanning electron microscopy (SEM) was applied to detect the external morphology of individual zircon grains. We used a JEOL JSM-6390LV equipped with a secondary electron detector for imaging (SEI) and an acceleration voltage of 20 or 30 kV. The specimens were coated with gold.

Laser Ablation Inductively Coupled Plasma Mass Spectrometry (LA-ICP-MS) on zircon

Isotopic concentrations of selected elements in zircon were determined by ICP-MS analyses using an AGILENT 7700 spectrometer after laser ablation with a CETAC LSX-213 laser system. The diameter of the ablated spots was 25 μm. The laser energy was set to 100 % of the maximum (100 %= 4 mJ at a spot diameter of 150 μm) at a laser pulse frequency of 10 Hz and 330 (for elemental concentrations) or 375 (for dating) laser pulses per analysis. A mixed helium and argon gas flow with 500 ml/min and 800 ml/min, respectively, served as carrier of the ablated material. The analyzed zircon grains had been mounted in epoxy resin after standard

Table 1: Selected EPMA analyses of minerals from the Požega granite (sample GV1) assemblage. The structural formulae were calculated on the basis of 8 O for feldspar and 3 O for hematite.

Mineral	**Pl**	**Kfs**	**Pl**	**Kfs**		**Hem**	**Hem**	**Hem**
Analysis	**#13**	**#10**	**#11**	**#12**		**#2**	**#4**	**#6**
SiO_2	67.70	65.87	68.34	64.92	TiO_2	8.40	7.15	7.34
TiO_2	0.01	0.02	0.01	0.00	Al_2O_3	0.40	0.12	0.42
Al_2O_3	19.79	18.53	20.09	18.38	Cr_2O_3	0.02	0.00	0.04
Fe_2O_3	0.14	0.15	0.33	0.12	FeO	7.48	6.37	6.48
Mn_2O_3	0.00	0.00	0.00	0.00	Fe_2O_3	83.04	84.47	83.76
MgO	0.00	0.01	0.00	0.00	MnO	0.07	0.06	0.10
CaO	0.72	0.02	0.71	0.02	MgO	0.00	0.00	0.01
Na_2O	11.36	2.47	11.01	0.51				
K_2O	0.27	13.45	0.39	16.15				
BaO	0.04	0.09	0.01	0.76				
Total	100.03	100.61	100.88	100.86	Total	99.42	98.17	98.15
Si	2.967	2.998	2.967	2.992	Ti	0.167	0.144	0.148
Ti	0.000	0.001	0.000	0.000	Al	0.012	0.004	0.013
Al	1.022	0.994	1.028	0.998	V	0.000	0.000	0.000
Cr	0.000	0.000	0.000	0.000	Cr	0.000	0.000	0.001
Fe^{3+}	0.005	0.005	0.011	0.004	Fe^{3+}	1.653	1.707	1.690
Mn^{3+}	0.000	0.000	0.000	0.000	sum6	1.833	1.856	1.852
Mg	0.000	0.000	0.000	0.000				
Ca	0.034	0.001	0.033	0.001	Fe^{2+}	0.165	0.143	0.145
Na	0.965	0.218	0.927	0.045	Mn	0.002	0.001	0.002
K	0.015	0.781	0.022	0.950	Mg	0.000	0.000	0.000
Ba	0.001	0.002	0.000	0.014	sum8	0.167	0.144	0.148
An	0.034	0.003	0.034	0.015				
Ab	0.951	0.218	0.944	0.045				
Or	0.015	0.780	0.022	0.941				

Table 2: Results of the whole-rock analyses of major (wt. %) and trace (ppm) elements with characteristic element ratios and Zr saturation temperatures after Watson & Harisson (1983) and Gervasoni et al. (2016) for selected Požega granite samples. The compositions were determined with ICP-MS and ICP-ES.

	GV4	GV5	GV6	GV2	GV1	GV3	d.l.	MIN	MAX	Mean	UCC
Major elements (wt. %)							**(wt. %)**				**McLennan (2001)**
SiO_2	67.61	67.79	69.78	70.12	71.49	72.61	0.01	67.61	72.61	69.90	66.00
TiO_2	0.65	0.66	0.51	0.52	0.29	0.28	0.01	0.28	0.66	0.49	0.68
Al_2O_3	16.04	16.40	15.73	15.10	14.58	14.07	0.01	14.07	16.40	15.32	15.20
Fe_2O_3	3.97	3.99	3.00	3.63	2.69	2.50	0.04	2.50	3.99	3.30	5.03
MnO	0.08	0.02	<0.01	0.02	0.03	<0.01	0.01	0.02	0.08	0.04	0.08
MgO	0.11	0.09	0.07	0.07	0.04	0.04	0.01	0.04	0.11	0.07	2.20
CaO	0.50	0.22	0.17	0.37	0.24	0.20	0.01	0.17	0.50	0.28	4.20
Na_2O	4.72	5.90	5.48	4.64	4.23	3.79	0.01	3.79	5.90	4.79	3.90
K_2O	3.83	2.41	3.68	3.46	4.96	4.99	0.01	2.41	4.99	3.89	3.40
P_2O_5	0.16	0.15	0.02	0.13	0.04	0.05	0.01	0.02	0.16	0.09	0.15
LOI	2.10	2.20	1.40	1.80	1.30	1.30	0.01	1.30	2.20	1.68	
Total	99.77	99.83	99.84	99.86	99.89	99.83		99.77	99.89	99.84	
Trace elements (ppm)							**(ppm)**				
As	7.2	17	6.1	7.8	7.2	7.9	0.5	6.1	17	8.8	
Au (ppb)	5.9	5.7	13	1.8	2.6	7.6	0.5 (ppb)	1.8	13	6.2	
Ba	430	307	574	439	519	679	1	307	679	491	550
Co	3.9	4.9	2.5	4.4	2.3	2.1	0.2	2.1	4.9	3.4	17
Cr	<14	<14	<14	<14	<14	<14	14	<14	<14	<14	83
Cs	11	2.6	4.1	5.2	2.9	2.9	0.1	2.6	11	4.8	5
Cu	9.4	0.7	2.0	4.7	7.7	3.5	0.1	0.7	9.4	4.7	25
Ga	23	23	22	21	19	19	0.5	19	23	21	17
Hf	16	16	13	17	10	9.1	0.1	9.1	17	14	5.8
Mo	0.5	0.3	0.6	0.5	0.8	0.6	0.1	0.3	0.8	0.6	
Nb	21	22	21	22	14	15	0.1	14	22	19	12
Ni	1.5	4.8	3.2	2.0	2.2	1.9	0.1	1.5	4.8	2.6	44
Pb	5.5	1.9	4.0	4.1	5.7	5.1	0.1	1.9	5.7	4.4	17
Rb	150	75	106	134	166	177	0.1	75	177	135	112
Sb	0.8	0.6	0.2	0.4	0.2	0.2	0.1	0.2	0.8	0.4	
Sc	6	7	5	6	3	3	1	3	7	5	13.6
Sn	10	14	5	10	9	7	1	5	14	9	
Sr	140	161	80	150	92	108	0.5	80	161	122	350
Ta	1.5	1.6	1.7	1.6	1.4	1.5	0.1	1.4	1.7	1.6	
Th	17	20	18	19	16	20	0.2	16	20	18	10.7
U	5.0	4.9	4.4	5.4	3.5	3.7	0.1	3.5	5.4	4.5	2.8
V	38	31	24	30	9	15	2	9	38	25	107
W	2.1	1.4	0.7	2.9	1.4	1.1	0.5	0.7	2.9	1.6	
Y	52	58	34	50	26	31	0.1	26	58	42	22
Zn	58	35	19	37	31	23	1	19	58	34	71
Zr	678	695	518	691	388	307	0.1	307	695	546	190
La	33	34	31	35	30	31	0.1	30	35	32	30
Ce	79	69	55	69	58	61	0.1	55	79	65	64
Pr	7.7	8.4	7.5	8.0	6.4	6.9	0.02	6.4	8.4	7.5	7.1
Nd	29	31	28	29	23	25	0.3	23	31	27	26
Sm	6.3	6.7	5.4	6.3	4.5	5.4	0.05	4.5	6.7	5.7	4.5
Eu	0.9	1.1	1.0	0.8	0.7	0.7	0.02	0.7	1.1	0.9	0.88
Gd	7.0	7.4	5.1	6.5	4.2	5.4	0.05	4.2	7.4	5.9	3.8
Tb	1.3	1.4	1.0	1.2	0.7	0.9	0.01	0.7	1.4	1.1	0.64
Dy	8.3	9.4	6.0	7.7	4.4	5.6	0.05	4.4	9.4	6.9	3.5
Ho	1.9	2.1	1.3	1.8	0.8	1.1	0.02	0.8	2.1	1.5	0.8
Er	5.9	6.7	4.2	5.6	2.8	3.5	0.03	2.8	6.7	4.8	2.3
Tm	0.9	1.0	0.7	0.9	0.5	0.6	0.01	0.5	1.0	0.8	0.33
Yb	6.3	7.0	4.5	5.9	3.2	3.8	0.05	3.2	7.0	5.1	2.2
Lu	1.0	1.1	0.7	0.9	0.5	0.6	0.01	0.5	1.1	0.8	0.32
MI	0.97	0.98	0.97	0.98	0.98	0.98		0.97	0.98	0.98	
A/CNK	1.25	1.29	1.18	1.25	1.14	1.17		1.14	1.29	1.21	
A/NK	1.35	1.33	1.20	1.33	1.18	1.21		1.18	1.35	1.27	
K_2O/Na_2O mol	0.53	0.27	0.44	0.49	0.77	0.87		0.27	0.87	0.56	
Ba/Rb	2.9	4.1	5.4	3.3	3.1	3.8		2.9	5.4	3.8	
10000·Ga/Al	2.69	2.63	2.65	2.67	2.51	2.55		2.51	2.69	2.62	
K/Ba	74	65	53	65	79	61		53	79	66	
K/Rb	212	267	288	215	247	234		212	288	244	
Rb/Nb	7.2	3.4	5.2	6.1	12.2	11.9		3.4	12.2	7.7	
Rb/Sr	1.1	0.5	1.3	0.9	1.8	1.6		0.5	1.8	1.2	
Sr/Y	2.7	2.8	2.3	3.0	3.5	3.5		2.3	3.5	3.0	
Y/Ho	27	27	26	28	31	27		26	31	28	
Y/Nb	2.5	2.6	1.7	2.3	1.9	2.1		1.7	2.6	2.2	
Zr/Hf	41	42	40	41	38	34		34	42	39	
$(La/Yb)_N$	3.59	3.25	4.56	3.96	6.20	5.58		3.25	6.20	4.52	
$(La/Sm)_N$	3.36	3.19	3.56	3.47	4.15	3.65		3.19	4.15	3.56	
$(Gd/Yb)_N$	0.89	0.85	0.91	0.90	1.06	1.15		0.85	1.15	0.96	
Ce/Ce*	1.19	0.99	0.87	0.99	1.02	1.01		0.87	1.19	1.01	
Eu/Eu*	0.44	0.47	0.55	0.39	0.50	0.42		0.39	0.55	0.46	
Σ REE	188	186	150	177	139	152		139	188	165	
M	1.28	1.24	1.32	1.23	1.32	1.26		1.24	1.32	1.28	
T_{WH} (°C)	944	950	909	950	878	859		859	950	915	
G	8.96	9.10	9.56	9.74	10.12	10.81		8.96	10.81	9.72	
T_G (°C)	927	935	894	950	875	830		830	950	899	

d.l.=detection limit; LOI=loss on ignition; MI (mafic index)=$FeO_T/(FeO_T+MgO)$; A/CNK=$Al_2O_3/(CaO+Na_2O+K_2O)$ in mol %; A/NK=$Al_2O_3/(Na_2O+K_2O)$; M (cation ratio)=$(Na+K+2Ca)/Al\cdot Si$; G=$(3\cdot Al_2O_3+SiO_2)/(Na_2O+K_2O+CaO+MgO+FeO)$ in molar proportions; T_{WH} and T_G – Zr saturation temperatures after Watson & Harisson (1983) and Gervasoni et al. (2016), respectively

procedures of extraction from granite (crushing of the rock, sieving, heavy-liquid separation, magnetic separation, and hand picking).

The data acquisition was performed using the Agilent Mass Hunter software (version B.01.01). Each analysis comprised the acquisition of the individual background ion intensities (gas-blank) for roughly 30 s followed by the acquisition of the ion intensities on laser irradiation of the sample spot for roughly 60 s. In the off-line data evaluation, the analytical signal of each ion was corrected by the subtraction of the corresponding averaged background intensity. Within a selected appropriate interval of the ablation time profile, the corrected individual ion intensities were integrated. This integral was divided by the integral of the corrected intensity of the selected isotope of the reference element. The software used for calibration and data evaluation was developed by J. Opitz (Massonne et al. 2013). In addition, Isoplot a geochronological toolkit for Microsoft Excel (Ludwig 2003) and IsoplotR, an open toolbox for geochronology (Vermeesch 2018), were used.

Zircon chemical analysis

As standards for the determination of elemental concentrations in zircon, DLH7 and DLH8 glasses from P&H Developments Ltd. and NIST612 and NIST610 glasses from National Institute of Standards and Technology, USA, were used. The validity of the calibration, data evaluation, and reproducibility were checked with the reference materials Diorite (DRN) and Zinnwaldite (ZW-C) from the Service d'Analyses des Roches et des Mineraux du CNRS. Lithium-borate glass disks of both were prepared using 0.6 g of powder of these reference materials and 3.6 g of lithium borate. Differently located ablation spots were used for analyses in order to check the homogeneity of the disks.

Relative elemental concentrations were calculated from the abundance of the corresponding isotope assuming natural isotopic distributions and individual calibration factors which were determined under the same experimental conditions. Absolute elemental concentrations were calculated on the basis of the known absolute elemental concentration of an internal reference element.

The following isotopes were monitored: ^{28,29}Si, ^{31}P, ^{42,44}Ca, ^{45}Sc, ^{49}Ti, ^{51}V, ^{52}Cr, ^{55}Mn, ^{56,57}Fe, ^{59}Co, ^{60}Ni, ^{66}Zn, ^{71}Ga, ^{88}Sr, ^{89}Y, ^{90,91}Zr, ^{93}Nb, ^{118}Sn, ^{137}Ba, ^{139}La, ^{140}Ce, ^{141}Pr, ^{146}Nd, ^{147,149}Sm, ^{151,153}Eu, ^{157}Gd, ^{159}Tb, ^{161,163}Dy, ^{165}Ho, ^{166}Er, ^{169}Tm, ^{172}Yb, ^{175}Lu, ^{177,178}Hf, ^{181}Ta, ^{208}Pb, ^{232}Th and ^{238}U. This selection excludes isobaric interferences with isotopes of other elements. In the case where two isotopes of one element were analyzed, very similar corresponding individual elemental concentrations were obtained, which shows the absence of significant matrix effects. This is emphasized especially for Fe, where the absence of a significant contribution of $[ArO]^+$ to the measured ion intensity at mass-to-charge ratio (m/z) 56 was confirmed. For this reason, the given values are the average of the corresponding individual elemental concentrations. While running the analyses, signals of laser ablation were stable for all elements. All elemental concentrations were calculated relative to the internal reference Zr=49.059 wt. % (see above). Therefore, the mean value of the two elemental Zr concentrations, as derived from the isotopes ^{90,91}Zr, was set to Zr=490590 ppm. The calculated elemental concentrations are summarized in Table 3. The concentrations of elements, which are usually not incorporated in zircon, were either very near to the detection limit or ascribed to inclusions in zircon.

U–Th–Pb geochronology

For dating, natural zircon reference materials FC1 (1099.0±0.6 Ma; Paces & Miller 1993), Peixe (564±4 Ma; Dickinson & Gehrels 2003 and 558±2.7 Ma; Shaulis et al. 2010), and Plešovice (337.13±0.37 Ma; Sláma et al. 2008) were used for isotopic corrections. The following masses were measured: ^{202}Hg, ^{204}(Hg+Pb), ^{206}Pb, ^{207}Pb, ^{208}Pb, ^{232}Th, ^{235}U, ^{238}U, and ^{254}UO.

In the off-line data evaluation, the analytical signal of each ion was treated by background correction and subsequent integration within an appropriate time interval as described before. Individual ages were calculated from the quotients of the radiogenic amounts of the isotopes ^{207}Pb/^{206}Pb, ^{206}Pb/^{238}U, ^{207}Pb/^{235}U, and ^{208}Pb/^{232}Th. To obtain the radiogenic amounts of these isotopes, two main corrections for the experimental intensities were considered: (1) a potential mass-dependent discrimination of the ions (the so-called mass bias), which affects all measured ion intensities, and (2) the subtractive correction of the contribution of non-radiogenic lead (common lead) as calculated from the amount of ^{204}Pb. Due to the overlap of ^{204}Hg and ^{204}Pb intensities, the contribution of ^{204}Hg was calculated from the measured ion intensity of ^{202}Hg assuming a natural isotope distribution of Hg. The contribution of common lead on ^{206,207,208}Pb was calculated from the ^{204}Pb intensity assuming a natural isotope distribution of Pb.

It must be emphasized that both corrections are based on an insignificant influence of the mass bias on the measured ion intensities. This mass bias was measured for the isotope distribution of Pb by laser ablation of a NIST612 glass. The obtained experimental isotope pattern reflected the natural isotope distribution within an accuracy of more than 99 %. Calibration was performed by ablating the reference zircons. For the correction of the intensity quotient ^{207}Pb/^{206}Pb only the mass bias was considered. This correction factor was set to 0.99. Correction factors for the experimental intensity quotients ^{206}Pb/^{238}U, ^{207}Pb/^{235}U, and ^{208}Pb/^{232}Th were obtained as the quotient of the corresponding concentration quotients calculated for the specific zircon age and the corresponding experimental intensity quotient. Inherently, these correction factors comprise a potential mass bias as well as the different element-specific sensitivity of the mass spectrometer. Individual calibration coefficients for ^{206}Pb/^{238}U, ^{207}Pb/^{235}U and ^{208}Pb/^{232}Th were obtained by averaging the corresponding results of the three reference materials. By dating these reference materials as unknowns with these averaged calibration coefficients,

Table 3: Chemistry of zircon from the Požega granite (sample GV1) determined by LA-ICP-MS with characteristic element ratios and detection limits (d.l.). Elemental mass concentrations and detection limits are given in ppm. b.d.l. – below detection limit. Normalization after Boynton (1984).

Element	Grain 1a	Grain 2a	Grain 3a	Grain 4a	Grain 5a	Grain 6a	Grain 7a	Grain 8a	Grain 9a	Grain 10a	Grain 11a	Grain 12a	Grain 13a	Grain 14a	Grain 15a	d.l.	MIN	MAX	Mean
Ba	8.8	0.4	0.3	21.5	5.0	0.3	1.1	0.4	0.5	2.8	13.3	1.2	0.4	1.7	0.9	0.2	0.3	21.5	3.9
Ca	4408	2387	4602	16631	1050	1724	4165	644	600	1774	5655	8773	2036	2072	4445	130	600	16631	4064
Cr	15	6.5	5.1	14	3.3	4.6	4.7	3.1	3.2	5.5	7.0	16	5.4	1.8	1.2	1	1.2	16.2	6.4
Fe	217	49	55	124	180	19	300	35	75	115	199	141	272	174	134	18	19	300	139
Ga	1.2	0.3	0.5	1.3	1.3	0.3	1.5	0.2	0.2	0.9	0.9	1.4	0.7	0.6	0.8	0.2	0.2	1.5	0.8
Hf	8870	9274	8602	8326	9312	9648	8234	8328	7127	8160	8543	12091	8494	10095	10002	0.1	7127	12091	9007
Mn	5.0	3.7	10	27	30	4.0	11	2.0	12	21	11	26	8.1	5.4	10	1	2	30	12
Nb	14	6.2	5.1	8.2	17	5.8	14	4.8	5.2	13	41	12	7.0	14	6.4	0.1	4.8	41	12
P	1278	814	2239	7649	1234	1116	2181	751	1062	738	1669	5127	1069	921	2070	34	738	7649	1995
Pb	18	6.1	5.3	12	16	5.4	14	6.2	6.3	16	25	12	6.8	26	10	0.1	5.3	26	12
Si	148470	133466	131335	151174	151092	137966	134385	139297	129644	153567	127439	155483	138988	146800	145758	157	127439	155483	141658
Sn	0.5	b.d.l.	b.d.l.	1.0	0.4	b.d.l.	0.3	b.d.l.	1.0	0.3	0.7	0.4	0.4	1.0	0.3	0.3	0.3	1.0	0.6
Sr	3.1	9.4	1.6	6.3	2.9	1.3	2.5	1.0	1.6	2.0	4.4	1.9	1.7	4.1	2.5	0.1	1.0	9	3
Ta	4.1	2.2	2.4	2.4	7.6	3.2	5.7	1.8	1.5	3.3	14	5.7	2.2	4.4	2.3	0.1	1.5	14	4.2
Th	704	336	292	467	709	295	796	369	268	688	1310	658	347	1096	487	0.1	268	1310	588
Ti	10934	3653	1200	7341	2376	3863	3032	893	964	6342	7753	1362	1544	4969	1383	1.5	893	10934	3841
U	828	433	442	645	1082	459	1186	478	365	769	1851	876	511	1266	652	0.1	365	1851	790
V	3.5	0.3	0.9	3.5	2.2	0.7	0.7	1.1	0.5	0.5	1.7	5.4	0.5	1.0	3.5	0.1	0.3	5.4	1.7
Y	5286	2687	2518	3625	4474	2281	4838	2609	2655	4104	6383	3777	2733	3237	3387	0.1	2281	6383	3640
Zn	11	5.3	3.6	8.2	8.2	4.8	7.5	3.6	4.7	5.7	7.3	4.1	3.1	11	9.3	0.8	3.1	11	6.5
Zr	490590	490590	490590	490590	490590	490590	490590	490590	490590	490590	490590	490590	490590	490590	490590	7	490590	490590	490590
La	23	8.2	33	85	2.7	6.7	8.4	2.6	4.3	0.8	4.9	82	9.5	1.8	27	0.01	0.8	85	20
Ce	112	32	95	249	43	36	60	34	23	39	79	280	36	36	140	0.02	23	280	86
Pr	6.6	2.3	8.9	20	1.1	2.0	2.8	1.3	1.2	0.6	2.2	23	2.8	0.7	9.6	0.01	0.6	23	5.7
Nd	42	14	51	120	11	14	20	11	10	10	19	133	18	7	53	0.08	7.1	133	35
Sm	34	13	21	45	17	14	22	13	10	20	30	51	14	14	31	0.10	10	51	23
Eu	2.7	1.2	1.5	3.1	1.8	1.5	1.4	1.8	1.1	1.2	2.8	3.9	1.1	1.2	3.5	0.03	1.1	3.9	2.0
Gd	138	66	69	120	92	66	109	69	47	109	152	146	69	80	97	0.10	47	152	95
Tb	45	23	21	35	32	20	35	23	16	40	49	43	23	29	32	0.01	16	49	31
Dy	603	300	259	444	434	268	469	303	211	591	633	558	306	352	349	0.07	211	633	405
Ho	192	95	85	149	144	89	157	97	71	207	204	171	100	128	122	0.01	71	207	134
Er	914	490	455	702	695	458	793	499	357	1059	1002	825	522	557	538	0.06	357	1059	658
Tm	165	90	85	116	127	86	143	90	69	200	182	146	101	120	105	0.01	69	200	122
Yb	1507	853	812	1058	1111	801	1310	826	638	1727	1683	1313	956	981	876	0.06	638	1727	1097
Lu	249	152	147	179	193	139	225	143	113	291	262	216	163	190	164	0.02	113	291	188
Th/U	0.85	0.77	0.66	0.72	0.66	0.64	0.67	0.77	0.73	0.89	0.71	0.75	0.68	0.87	0.75		0.64	0.89	0.74
U/Yb	0.55	0.51	0.54	0.61	0.97	0.57	0.90	0.58	0.57	0.45	1.10	0.67	0.53	1.29	0.74		0.45	1.29	0.71
Zr/Hf	55	53	57	59	53	51	60	59	69	60	57	41	58	49	49		41	69	55
Ce_N/Yb_N	0.02	0.01	0.03	0.06	0.01	0.01	0.01	0.01	0.01	0.01	0.01	0.06	0.01	0.01	0.04		0.01	0.06	0.02
Ce_N/Sm_N	0.79	0.59	1.09	1.34	0.61	0.62	0.66	0.63	0.56	0.47	0.64	1.32	0.62	0.62	1.09		0.47	1.34	0.78
Ce/Ce*	2.19	1.77	1.33	1.45	6.01	2.37	2.98	4.45	2.44	13.55	5.79	1.55	1.68	7.72	2.09		1.33	13.55	3.82
Eu/Eu*	0.12	0.13	0.12	0.13	0.14	0.15	0.09	0.18	0.16	0.08	0.13	0.14	0.11	0.11	0.20		0.08	0.20	0.13
Eu_N/Yb_N	0.01	0.00	0.01	0.01	0.00	0.01	0.00	0.01	0.00	0.00	0.00	0.01	0.00	0.00	0.01		0.00	0.01	0.01
Gd_N/Yb_N	0.07	0.06	0.07	0.09	0.07	0.07	0.07	0.07	0.06	0.05	0.07	0.09	0.06	0.07	0.09		0.05	0.09	0.07
La_N/Yb_N	0.01	0.01	0.03	0.05	0.00	0.01	0.00	0.00	0.00	0.00	0.00	0.04	0.01	0.00	0.02		0.00	0.05	0.01
La_N/Sm_N	0.43	0.40	0.99	1.19	0.10	0.30	0.24	0.13	0.27	0.03	0.10	1.01	0.43	0.08	0.55		0.03	1.19	0.42
Sum REE	4032	2139	2145	3326	2906	2000	3357	2115	1570	4295	4306	3990	2322	2497	2547		1570	4306	2903
Sum oxides (wt %)	103.20	97.77	97.44	105.94	101.70	98.72	98.89	98.18	95.98	102.81	98.75	104.78	98.59	101.23	100.87		95.98	105.94	100.32

the averaged individual ages of the three reference materials were corroborated by their literature values (Table 4).

The precise common lead correction turned out to be problematic especially for zircon younger than 600 Ma and for zircon with small amounts of uranium and thorium. In these cases the mass spectrometer used does not provide the necessary precision for the detection of the ion intensity at m/z 204. Furthermore, the $^{207}Pb/^{206}Pb$ age is very sensitive to changes of ^{204}Pb, whereas the $^{206}Pb/^{238}U$ age is only slightly affected. Therefore, an optimization of the ^{204}Pb intensity was applied, which varies the ^{204}Pb intensity until the $^{207}Pb/^{206}Pb$ age reaches the $^{206}Pb/^{238}U$ age. During this optimization of ^{204}Pb, the $^{206}Pb/^{238}U$ averaged age changes only for 0.6 Ma, which is within the given error limit of the mean value, and thus confirms the applicability of the common lead correction method. This makes the $^{206}Pb/^{238}U$ age the most reliable. This method (applied also in Martínez et al. 2020) is an improvement of the usual static extrapolation method in the Tera-Wasserburg plot of the radiogenic intensity quotients $^{207}Pb/^{206}Pb$ versus $^{238}U/^{206}Pb$.

X-ray diffraction

XRD analysis of the granite samples was performed with a PHILIPS PW304/60 X' Pert PRO diffractometer with θ–θ geometry. The instrument is equipped with an X'celerator detector using CuKα radiation ($K\alpha_1$=1.54060 Å, $K\alpha_2$=1.54443 Å) from a tube operated at 40 kV and 40 mA. Continuous scanning with the step size of 0.02° 2θ/sec was performed for the 4 to 120° (2θ) interval.

Results

Outcrop and rock descriptions

The main outcrop of the Požega granite is a small abandoned quarry (Fig. 2a; 45.30270°N, 17.64142°E), approximately 50 m wide, near the road from Požega to the village of Gradski Vrhovci, just before entering the village. All samples were collected either in the quarry or within a distance of 300–400 m around the quarry. The Požega granite samples are reddish to pale-pinkish in colour and massive with a fine- to medium-grained granitic texture (1–2 mm) and mainly composed of alkali feldspar (perthite, ca. 65 vol. %) and quartz (25–30 vol. %) – (Fig. 2b), with small amounts of separate albite grains and hematite (up to 2–3 vol. % each). Zoned feldspar grains are composed of a sericitized inner core with twin lamellae overgrown by unaltered perthite. Quartz-alkali feldspar intergrowths and micrographic textures are common. Accessory minerals include zircon, apatite, hematite, and monazite. Chalcopyrite and a clay mineral similar to smectite were found as secondary minerals.

Mineral chemistry

Chemical analyses of the mineral constituents from sample GV1 (selected as a representative sample of Požega granite; Figs. 2b and 3a–d) are given in Table 1. In the analyzed thin-sections of 6 granite samples most minerals show uniform compositions with the exception of hematite that comprises exsolution lamellae of ilmenite not wider than 1–2 μm (Fig. 3b, Table 1). Therefore, this phase shows apparently a wider compositional range depending not only on the location of the analytical spot but also on the EPMA beam width.

EPMA analyses of feldspar demonstrate that most grains are perthite with Na-rich domains composed of albite (X_{Ab}=0.94–0.95). The compositions of the potassium-rich domains are between X_{Or}=0.78 and 0.94 (Table 1). Isolated grains of pure albite are present but rare.

Whole-rock chemistry

According to the modal composition using the IUGS classification (Streckeisen 1974), the rock studied is alkali-feldspar granite (Fig. 4a) which is compatible with the whole-rock major-element classification after De la Roche et al. (1980: alkali granite in Fig. 4b). The Požega granite (Table 2) is characterized by: (1) highly siliceous compositions (SiO_2 between 67.6 and 72.6 wt. %), (2) high abundances of alkalies (Fig. 4a: K_2O+Na_2O between 8.1 and 9.2 wt. % with K_2O up to 5.0 wt. %), (3) relatively high K_2O/Na_2O molar ratios (0.27–0.87), (4) high Al_2O_3 abundances (14.1–16.4 wt. %, A/CNK ratios=$Al_2O_3/(CaO+Na_2O+K_2O)$ between 1.14 and 1.29 mol %, A/NK ratios=$Al_2O_3/(Na_2O+K_2O)$ of 1.18–1.35), and (5) low CaO (0.17–0.50 wt. %), MgO (0.04–0.11), and MnO (<0.08) abundances and relatively high Fe_2O_3 contents (2.5–4.0 wt. %). Thus, FeO_T/FeO_T+MgO ratios (0.97–0.98) and normative corundum and hematite (both are up to 4.0 wt. %) are high. There is no normative diopside. These parameters indicate that the rocks studied refer to a peraluminous, ferroan,

Table 4: Natural zircon references treated as unknowns: $^{206}Pb/^{238}U$, $^{207}Pb/^{235}U$, and $^{208}Pb/^{232}Th$ ages, n=number of measurements.

Natural zircon reference materials	FC1 1099.0 ± 0.6 Ma (Paces & Miller 1993)			Peixe 564 ± 4 Ma (Dickinson & Gehrels 2003) 558 ± 2.7 Ma (Shaulis et al. 2010)			Plešovice 337.13±0.37 Ma (Sláma et al. 2008)		
	n=7			n=6			n=5		
	$^{206}Pb/^{238}U$	$^{207}Pb/^{235}U$	$^{208}Pb/^{232}Th$	$^{206}Pb/^{238}U$	$^{207}Pb/^{235}U$	$^{208}Pb/^{232}Th$	$^{206}Pb/^{238}U$	$^{207}Pb/^{235}U$	$^{208}Pb/^{232}Th$
Weighted average (Ma)	1104	1111	1144	549	564	563	339	329	320
Error 2σ (Ma)	19.0	21.0	20.0	8.3	11.0	12.0	7.2	7.8	8.4
MSWD	7.0	1.0	5.5	1.9	0.9	4.2	1.0	0.6	6.4

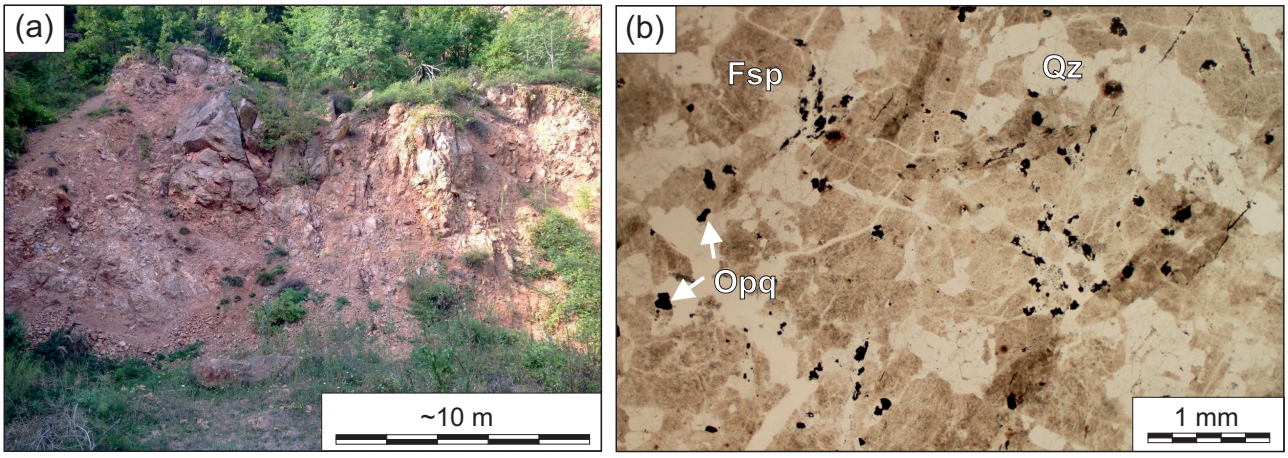

Fig. 2. (a) The small quarry which is the main outcrop of the Požega granite and **(b)** plain-polarized transmitted-light photomicrograph of a typical micro-fabric of the Požega granite taken from a thin section of the Gradski Vrhovci sample (GV1) with the following assemblage: Qz — quartz; Fsp — feldspar (perthite); Opq — opaque mineral (hematite). Abbreviations after Whitney & Evans (2010).

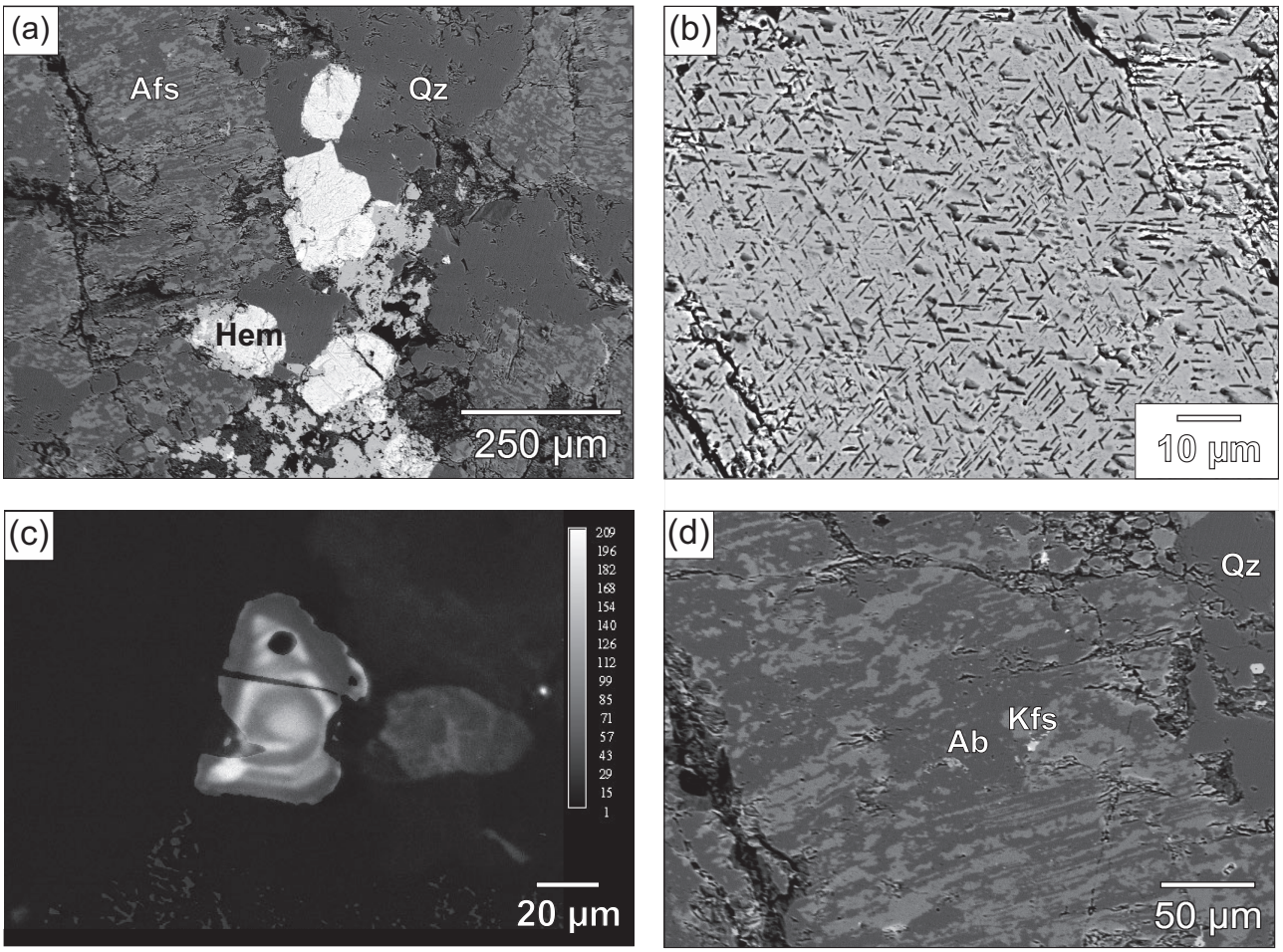

Fig. 3. BSE images of **(a)** the texture of the Požeška granite (sample GV1); Afs — alkali feldspar, Hem — hematite, Qz — quartz; **(b)** hematite with crystallographically oriented ilmenite exsolution; **(c)** CL image of zircon showing oscillatory zoning; **(d)** perthite; Ab — albite, Kfs — K-feldspar, Qz — quartz.

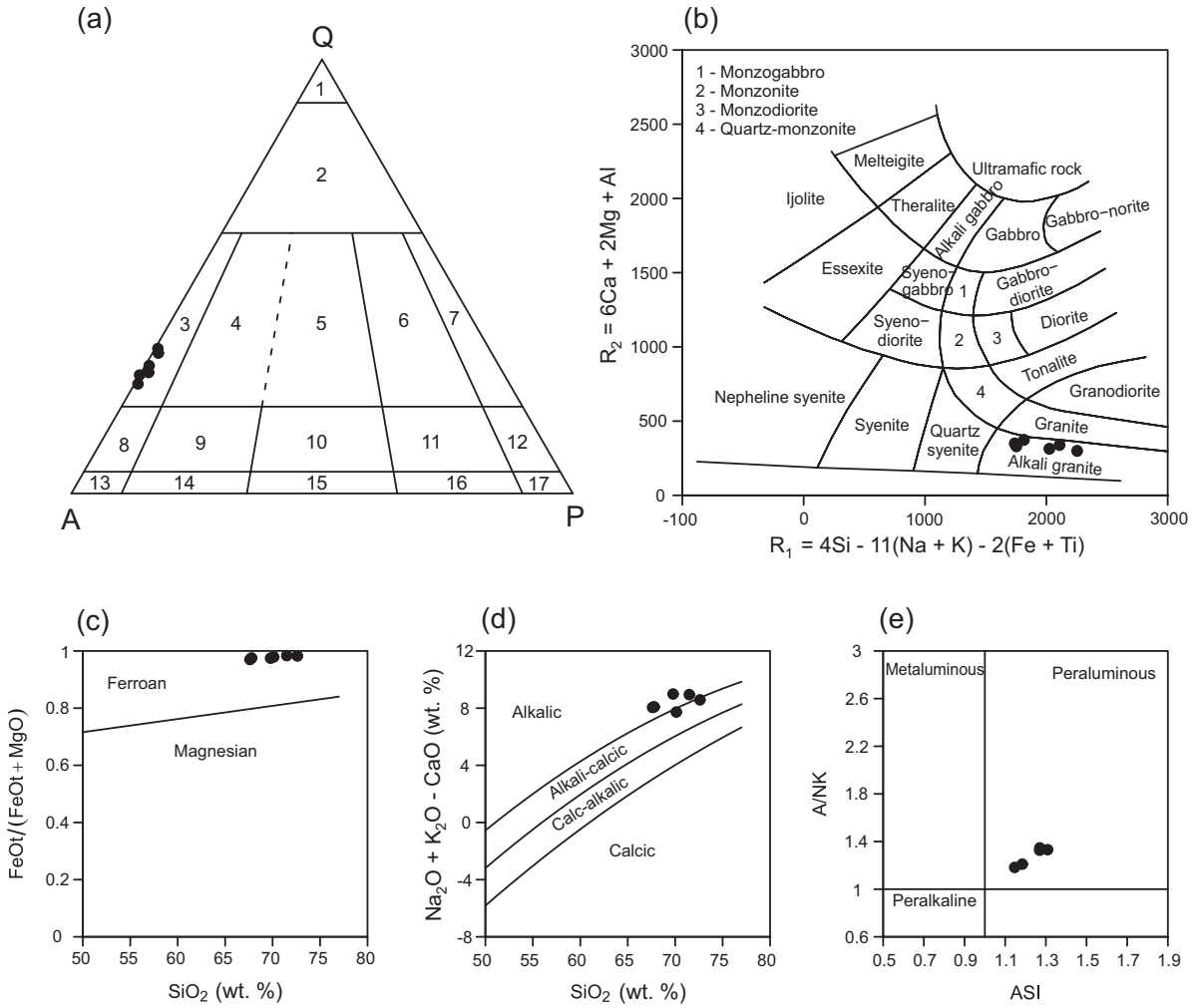

Fig. 4. (a) QAP modal composition diagram after Streckeisen (1974): Q — quartz, A — alkali feldspar, P — plagioclase, 1 — quartzolite, 2 — Q-rich granite, 3 — alkali-feldspar granite, 4 — syenogranite, 5 — monzogranite, 6 — granodiorite, 7 — tonalite, 8 — Q-alkali-feldspar syenite, 9 — Q-syenite, 10 — Q-monzonite, 11 — Q-monzodiorite/Q-monzogabbro, 12 — Q-diorite/Q-gabbro/Q-anorthosite, 13 — alkali-feldspar syenite, 14 — syenite, 15 — monzonite, 16 — monzodiorite/monzogabbro, 17 — diorite/gabbro. Classification and discrimination diagrams based on major elements for granite samples from Mt. Požeška Gora after (**b**) De la Roche et al. (1980), and (**c–e**) Frost et al. (2001) and Frost & Frost (2011).

alkali–calcic to alkalic geochemical characteristics (Fig. 4c–e). Chemical compositions of the samples analyzed in this study (Table 2) are comparable with the chemical data of the limited set of elements presented by Pamić (1987) for the "Gradski Vrhovci granites".

In the primitive mantle-normalized element plot (Fig. 5a), the analyzed granite samples display positive anomalies of K, Pb, and Zr and relatively pronounced negative anomalies of the high field-strength elements (HFSEs), Nb, P, and Ti as well as of Ba and Eu. Chondrite-normalized REE data (Fig. 5b) reveal an enrichment of light rare-earth elements (LREE) relative to heavy rare-earth elements (HREE) with $(La/Yb)_N$, $(La/Sm)_N$ and $(Gd/Yb)_N$ ranging from 3.3 to 6.2, 3.2 to 4.2, and 0.9 to 1.2, respectively. Eu/Eu* is 0.4–0.6, whereas Ce/Ce* is 0.9–1.2. The sum of REE is 139–188 ppm. Sr/Y ratios range between 2.3 and 3.5. Contents of Y and Yb are 26–58 ppm and 3.2–7.0 ppm, respectively.

Zircon

External morphology and internal structure

Zircon was separated from sample GV1. The analyzed populations of zircon consist in total of 184 generally small grains being 60–75 μm long and 25–35 μm thick. Aspect ratios range from 1.7:1 to 2.9:1, with the median value of 2.2:1. The external morphology is governed by {100} prisms and {101}>>{211} bipyramids. Types D (50 % of total population), J5 (30 %), and J4 (11 %) after Pupin's (1980) zircon typology method (Fig. 6a,b) prevail. Such morphologies are considered to characterize zircon crystallized from magma with lower crust/upper mantle origin (Pupin & Turco 1972; Pupin 1980).

The zircon grains are colourless to slightly yellowish with high transparency and birefringence and they are included in the late-crystallized minerals K-feldspar and quartz. Some

zircon grains include hematite, apatite and a needle-like mineral (see following section). CL and BSE images of several zircon grains reveal clear signs of oscillatory zoning (Fig. 3c), typical of magmatic growth.

Inclusions in zircon

Aside from hematite (bands at 223, 290, 409, 498, 609 and 1313 cm^{-1}, strongest at 290 and 409 cm^{-1}, after Frezzotti et al. 2012) and apatite (432, 449, 581, 592, 608, 965, 1042, 1053 and 1081 cm^{-1}, strongest at 965 cm^{-1}; bands at 3100–3800 cm^{-1} characteristic for OH, after Frezzotti et al. 2012), the Raman spectra of inclusions (<10 μm in size) in zircon (Fig. 7) indicate the presence of kokchetavite (110, 391 and 835 cm^{-1}, strongest at 391 and 835 cm^{-1}, after Kanzaki et al. 2012) and kumdykolite (154, 222, 265, 407, 464 and 492 cm^{-1}, strongest at 222 and 492 cm^{-1}, after Kotková et al. 2014). The latter two minerals are polymorphs of $KAlSi_3O_8$ and $NaAlSi_3O_8$, respectively, representing metastable phases in melt inclusions as a consequence of rapid crystallization (Ferrero & Angel 2018). The characteristic bands of zircon after Frezzotti et al. (2012) are at 202, 212, 225, 356, 392, 438, 972–974 and 1005–1008 cm^{-1} (strongest at 356, 972–974 and 1005–1008 cm^{-1}). Raman bands of zircon, despite the confocal mode, are very intense, making the identification of included phases difficult. Some of the phases that might be expected to be present (e.g., possible finding of cristobalite that together with kokchetavite and kumdykolite may represent former melt inclusions; e.g., Ferrero & Angel 2018) have not been identified yet.

However, it should be noted that some Raman bands in the obtained spectra correspond to bands of anatase (143, 195, 395, 514 and 638 cm^{-1}, strongest at 143 and 638 cm^{-1}, after Frezzotti et al. 2012). Furthermore, a few zircon grains enclose undefined needles of solid inclusions. Such zircon grains were analyzed (LA-ICP-MS) with a relatively large laser diameter of 25 μm that covers almost the entire prism face of the analyzed mineral. Results obtained this way show elevated concentrations of titanium (Table 3) followed by low Fe concentrations that fit neither zircon nor ilmenite. Thus, it is a reasonable assumption that such needle-like inclusions could represent a Ti-phase. Titanium dioxide occurs in nature as rutile, anatase and brookite with rutile being the high-temperature and high-pressure phase relative to anatase, whereas brookite is often considered to be of secondary origin (Dachille et al. 1968; Fu et al. 2013). Thus, rutile is a plausible candidate for the needle-like Ti-phase.

Zircon chemical analysis

All analyzed zircon from a single sample of the Požega granite (GV1) shows variable uranium (365–1851 ppm) and thorium (268–1310 ppm) contents (Table 3), with Th/U ratios ranging from 0.64 to 0.89, consistent with a magmatic origin (Hoskin & Schaltegger 2003). According to the chemical composition (high U_{mean}=790 ppm and Th_{mean}=588 ppm, Th/U=0.74, Zr/Hf=55) it is likely that these zircon grains crystallized in a deep magma chamber at relatively high and constant temperature (Wang et al. 2010). The U/Yb ratio (mean 0.71) and Y contents (mean 3640 ppm) are consistent with a crustal environment for melt generation.

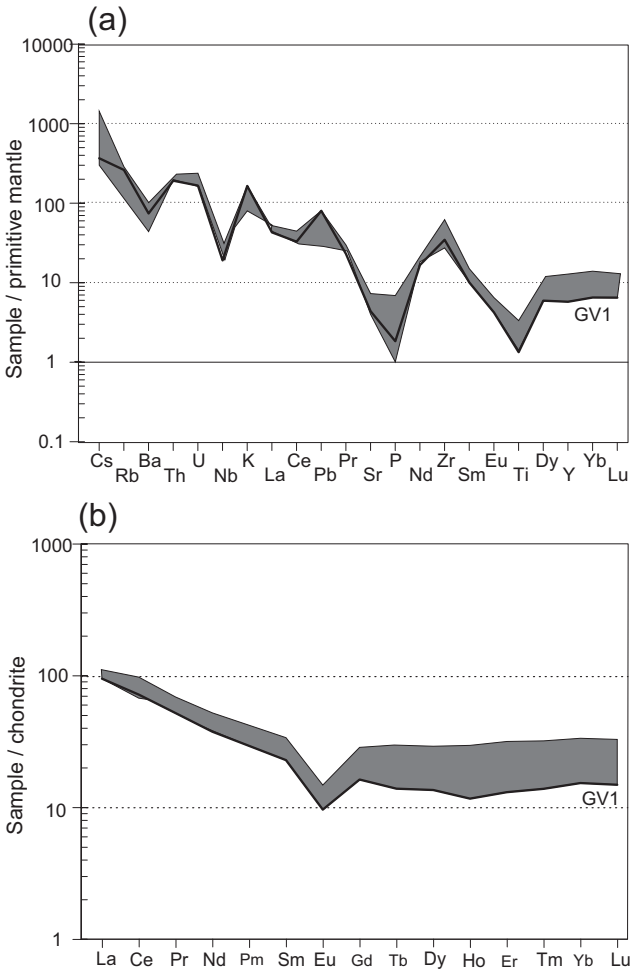

Fig. 5. Primitive mantle-normalized element diagram **(a)** and chondrite-normalized REE patterns **(b)** for samples of granite from Mt. Požeška Gora using normalizing factors after Sun & McDonough (1989) and Boynton (1984), respectively. Sample GV1, from which zircon grains were separated, is marked by a bold line.

The geochemical patterns of separated zircon grains, summarized in primitive-mantle-normalized and chondrite-normalized (REE) diagrams (Fig. 8a,b) show similar anomalies to those of the host rock (i.e. positive U, Pb, and Zr anomalies and negative Ba, Ti, and Eu anomalies) implying that only one generation of zircon is present. The patterns are typical for igneous zircon (Belousova et al. 2002) and are characterized by: (1) average values of $(La/Yb)_N$=0.01 and ΣREE=2903 ppm, (2) steeply positive patterns enriched in HREE ($(Gd/Yb)_N$=0.07) relative to the moderately fractionated LREE ($(La/Sm)_N$=0.42), (3) a variability in the degree of LREE enrichment, (4) a positive Ce-anomaly (Ce/Ce*=3.82), and (5) moderate to pronounced negative Eu-anomalies (Eu/Eu*=0.13). In only a few cases, the positive Ce anomaly was less pronounced possibly resulting from alteration of zircon.

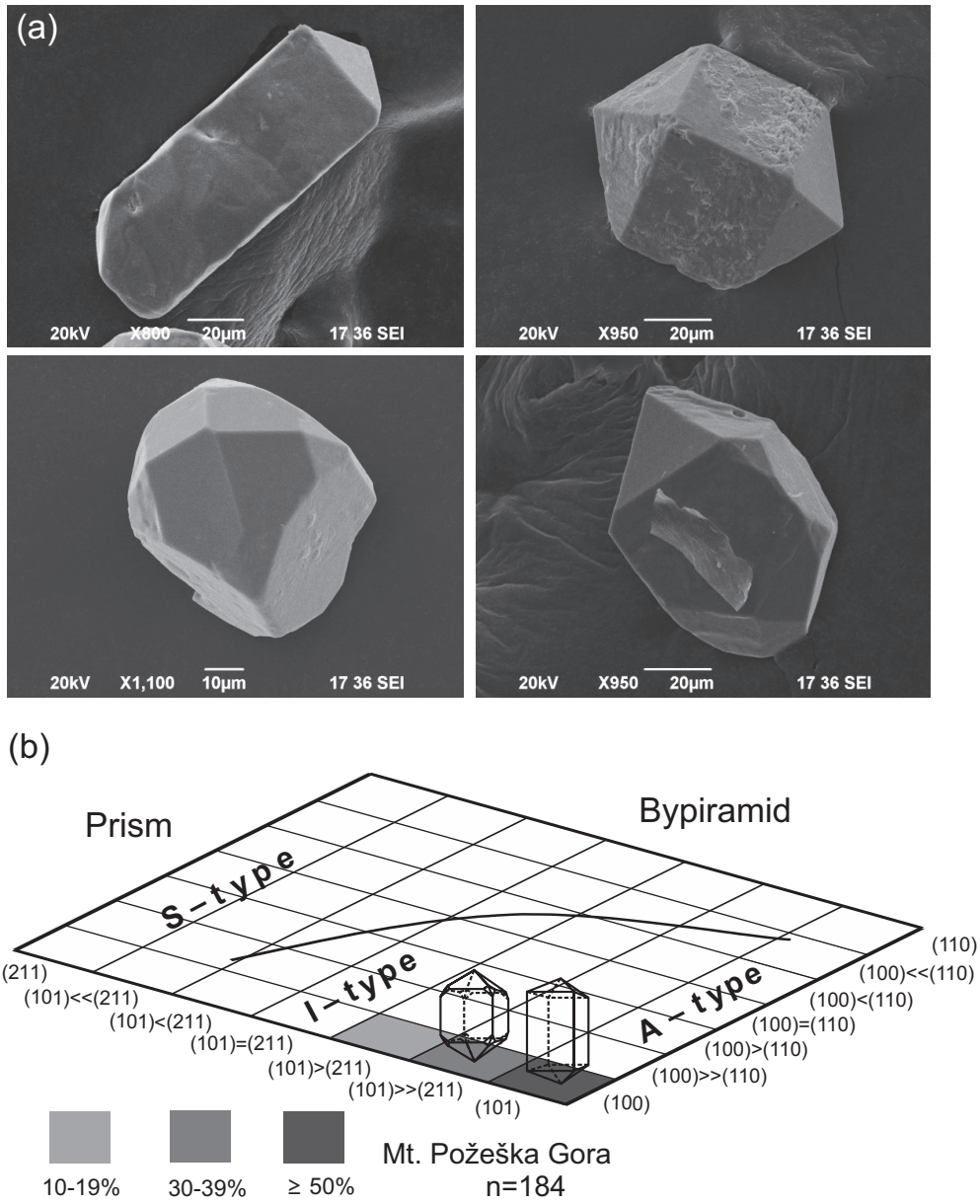

Fig. 6. (a) Typical external morphologies of zircon from the Požega granite (sample GV1) and (**b)** morphologies and types of investigated zircon grains shown on the modified zircon typology diagram after Pupin (1980).

U–Th–Pb geochronology

All 19 zircon grains selected for geochronology are of igneous origin; they are characterized in particular by high transparency, euhedral shape, and oscillatory zonation. The U–Th–Pb analytical results for zircon are given in Table 5 and displayed in a concordia diagram in Fig. 9. A concordia age of 83.6±1.5 Ma and a mean square weighted deviation (MSWD) of 1.9 were obtained. Zircon ages resulting from individual calibrated quotients of isotopic intensities are 82.9±1.8 Ma ($^{206}Pb/^{238}U$), 85.4±3.0 Ma ($^{207}Pb/^{235}U$) and 86.2±2.5 Ma ($^{208}Pb/^{232}Th$) with errors given as 2σ values. Within these errors, the three ages coincide. The $^{206}Pb/^{238}U$ age of 82.9±1.8 Ma is considered to be the most reliable age (see section Laser Ablation Inductively Coupled Plasma Mass Spectrometry (LA-ICP-MS) on Zircon – U–Th–Pb geochronology).

The MSWD value of 3.3 for $^{206}Pb/^{238}U$ might be interpreted as the result of the presence of slightly different age (sub) groups. However, the MSWD values of 0.46 and 0.82 for $^{207}Pb/^{235}U$ and $^{208}Pb/^{232}Th$, respectively, are in support of a single zircon generation.

Geothermometry

Temperatures of the saturation of the magma with Zr and zircon crystallization were calculated (Watson & Harrison 1983) using whole-rock Zr concentrations obtained by ICP-MS.

Calculations of these temperatures (Table 2) yielded values of 860–950 °C, indicating a high-temperature environment. A similar temperature range of 830–950 °C was calculated using the calibration by Gervasoni et al. (2016).

Discussion

General geochemical characteristics and classification of the Požega granite

The Požega granite is a leucocratic alkali-feldspar granite characterized by relatively high contents of SiO_2, Al_2O_3, and total alkalies, low contents of CaO, MgO, and MnO, and high FeO_T/FeO_T+MgO ratios. According to the geochemical classification proposed for granitic rocks by Frost et al. (2001) and the diagrams presented in Fig. 4c–e, the magma from which the Požega granite crystallized was ferroan, alkalic to alkali–calcic and peraluminous.

The minor and trace element signatures of the Požega granite are typical for an A-type granite after Collins et al. (1982), Whalen et al. (1987), Eby (1990, 1992) and King et al. (1997). They are characterized by relatively high contents of HFSE (Y, Nb, Zr, Ga, Ta, U, Th). LILE are significantly enriched with respect to the primitive mantle with positive anomalies of Th, K, and Zr and negative anomalies of Ba, Nb, P, Eu, and Ti (Fig. 5a,b). When compared with other types of granite, especially I- and S-types, A-type granites are characterized by high FeO* (>1 wt. %), K, HFSE, and total REE contents and a 10000·Ga/Al ratio of 2.5–2.7. In addition, they show low MgO, CaO, Cr, Ni, Sr, and Ba abundances (Collins et al. 1982; Eby 1990; King et al. 1997). These characteristics are consistent with the geochemical signature of the Požega granite (Fig. 5, Table 2). Whalen et al. (1987) used a wide range of geochemical data from the literature to develop a series of discrimination diagrams for A-type granites. On all these diagrams the Požega granite samples fall in the field of the A-type granite (Fig. 10).

Following the rationale of Eby (1992), A-type granites can be further subdivided into A_1 and A_2 subtypes. Granitoids that belong to the group A_1 are interpreted as differentiates of basaltic magma derived from an ocean-island basalt (OIB)-like source (with OIB-like signature). They are associated with true anorogenic (within-plate) settings, which are generally separated from periods of compressional tectonics by 50 to 100 Ma or even more. A_1-subtype granitoids are most likely the result of significant horizontal crustal extension (for review see Grebennikov 2014). Emplacement of igneous rocks in such a setting is related to the relatively unobstructed ascent of mantle melts or plumes. These rocks show minor contamination by crustal material, because in the case of brittle deformation and cold crust (classical continental rifting), the interaction of mantle magmas with crustal material is suppressed. However, if any event stops the ascent of these melts in deep crustal levels, significant contamination can occur to produce the A_1-type signature.

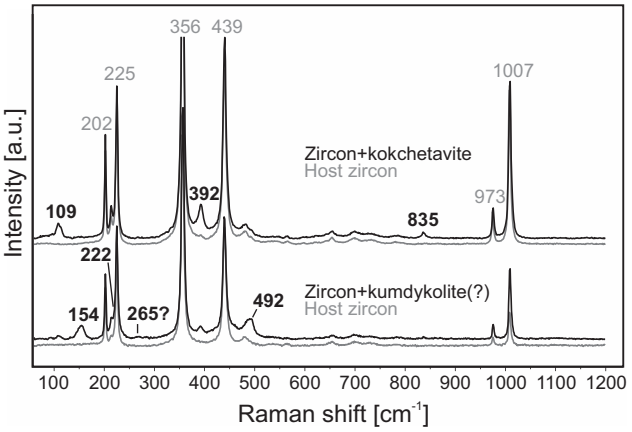

Fig. 7. Raman spectra of kokchetavite and kumdykolite(?) inclusions in zircon. Spectra were compared with data given by Kanzaki et al. (2012), Kotková et al. (2014), and Ferrero et al. (2016). No bands related to O–H stretching are visible in the kokchetavite spectrum so that the presence of K-cymrite (Kanzaki et al. 2012) can be excluded.

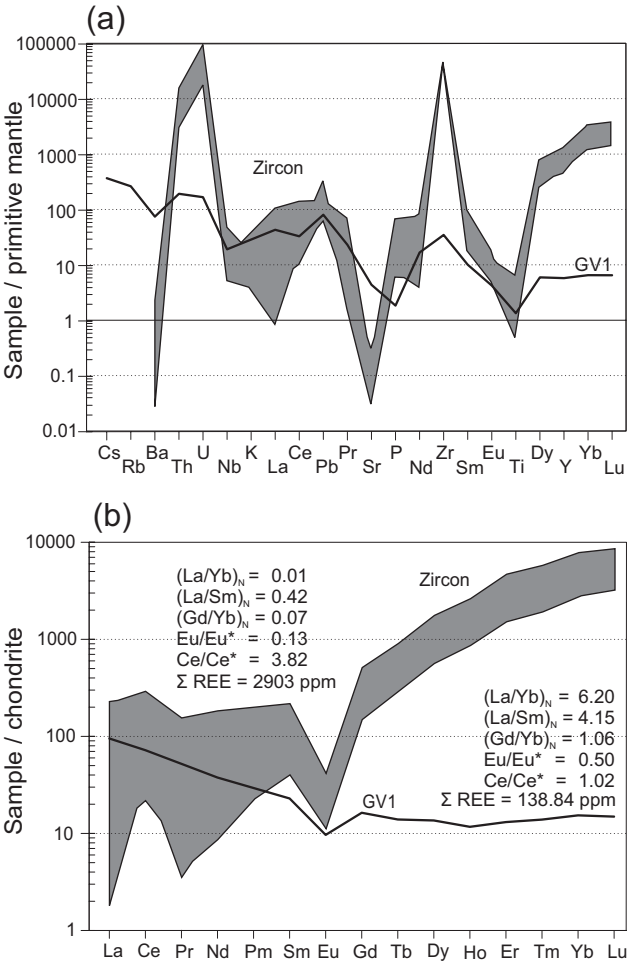

Fig. 8. Primitive mantle-normalized element diagram **(a)** and chondrite-normalized REE patterns **(b)** for zircon grains separated from the Požega granite (sample GV1) using normalizing factors after Sun & McDonough (1989) and Boynton (1984), respectively. Results of the whole-rock analysis of GV1 (thick line) are given for comparison.

Table 5: Individual elemental and isotopic concentrations and ages of zircon from the Požega granite (sample GV1) obtained from calibrated isotopic ratios of $^{206}Pb/^{238}U$, $^{207}Pb/^{235}U$, and $^{208}Pb/^{232}Th$. Elemental concentration of Pb refers to the sum of all Pb isotopes.

Grain	Elemental concentrations (%)						Isotopic concentrations (ppm)		
	Si	Zr	Th	U	Pb (ppm)	Th/U	^{206}Pb	^{207}Pb	^{208}Pb
1b	15.43337	49.05900	0.04573	0.05280	7.90	0.87	5.73	0.45	1.70
2b	15.31893	49.05900	0.05017	0.06335	10.41	0.79	8.08	0.51	1.82
3b	14.85277	49.05900	0.06865	0.08914	16.31	0.77	12.55	0.88	2.87
4b	15.18199	49.05900	0.09656	0.14573	25.44	0.66	19.65	1.53	4.22
5b	15.23803	49.05900	0.06843	0.08375	15.41	0.82	11.69	0.93	2.77
6b	14.20939	49.05900	0.05839	0.06817	10.34	0.86	8.02	0.46	1.85
7b	14.65993	49.05900	0.05157	0.06474	9.04	0.80	7.11	0.37	1.57
8b	14.21588	49.05900	0.04095	0.05160	7.20	0.79	5.45	0.37	1.38
9b	14.78252	49.05900	0.05592	0.05733	9.36	0.98	6.89	0.50	1.95
10b	14.97827	49.05900	0.05866	0.06792	11.50	0.86	8.33	0.69	2.46
11b	15.04390	49.05900	0.07495	0.09216	15.66	0.81	11.57	0.96	3.12
12b	15.00371	49.05900	0.14386	0.14951	24.85	0.96	19.18	0.99	4.66
13b	14.84675	49.05900	0.05908	0.07222	10.63	0.82	8.17	0.54	1.92
14b	14.76493	49.05900	0.03516	0.05259	7.10	0.67	5.61	0.35	1.13
15b	15.01917	49.05900	0.09600	0.12021	18.65	0.80	14.47	0.94	3.22
16b	14.56898	49.05900	0.18472	0.20819	38.75	0.89	29.15	2.13	7.42
17b	15.14385	49.05900	0.08230	0.11101	17.50	0.74	14.02	0.78	2.70
18b	15.26086	49.05900	0.08564	0.09884	16.29	0.87	12.86	0.74	2.68
19b	14.71267	49.05900	0.03595	0.04492	6.44	0.80	5.06	0.27	1.11

Grain	Isotopic ratios						Age (Ma)					
	$^{206}Pb/^{238}U$	1σ	$^{207}Pb/^{235}U$	1σ	$^{208}Pb/^{232}Th$	1σ	$^{206}Pb/^{238}U$	1σ	$^{207}Pb/^{235}U$	1σ	$^{208}Pb/^{232}Th$	1σ
1b	0.01166	0.00049	0.08294	0.00451	0.00406	0.00032	74.7	3.1	80.9	4.4	82.0	6.5
2b	0.01319	0.00039	0.09216	0.00604	0.00424	0.00027	84.5	2.5	89.5	5.9	85.8	5.5
3b	0.01527	0.00110	0.09940	0.01177	0.00468	0.00032	97.7	7.0	96.2	11.4	94.7	6.5
4b	0.01496	0.00058	0.09519	0.00923	0.00419	0.00055	95.7	3.7	92.3	9.0	84.8	11.1
5b	0.01497	0.00062	0.09771	0.00847	0.00400	0.00025	95.8	4.0	94.7	8.2	80.9	5.1
6b	0.01295	0.00058	0.08715	0.00505	0.00420	0.00019	83.0	3.7	84.8	4.9	85.0	3.9
7b	0.01275	0.00053	0.08795	0.00412	0.00427	0.00017	81.7	3.4	85.6	4.0	86.3	3.5
8b	0.01147	0.00048	0.07867	0.01024	0.00397	0.00038	73.5	3.1	76.9	10.0	80.3	7.8
9b	0.01292	0.00065	0.08597	0.00733	0.00415	0.00031	82.8	4.2	83.7	7.1	83.9	6.2
10b	0.01310	0.00118	0.09078	0.01729	0.00432	0.00077	83.9	7.5	88.2	16.8	87.4	15.6
11b	0.01340	0.00063	0.08760	0.01060	0.00411	0.00033	85.8	4.0	85.3	10.3	83.1	6.7
12b	0.01423	0.00111	0.09180	0.00760	0.00459	0.00013	91.1	7.1	89.2	7.4	92.8	2.7
13b	0.01232	0.00071	0.08014	0.00845	0.00383	0.00031	78.9	4.5	78.3	8.3	77.5	6.3
14b	0.01167	0.00061	0.08099	0.00814	0.00385	0.00034	74.8	3.9	79.1	8.0	77.9	6.8
15b	0.01313	0.00148	0.08590	0.01112	0.00396	0.00049	84.1	9.5	83.7	10.8	80.2	10.0
16b	0.01514	0.00120	0.09485	0.01769	0.00446	0.00053	96.9	7.7	92.0	17.2	90.2	10.8
17b	0.01393	0.00096	0.09264	0.00581	0.00435	0.00055	89.2	6.1	90.0	5.6	87.9	11.1
18b	0.01432	0.00098	0.09317	0.00866	0.00407	0.00032	91.7	6.3	90.4	8.4	82.3	6.4
19b	0.01246	0.00033	0.08547	0.00351	0.00427	0.00025	79.8	2.1	83.3	3.4	86.3	5.1
Weighted average (Ma)							**82.9**		**85.4**		**86.2**	
Error 2σ (Ma)							1.8		3.0		2.5	
MSWD							3.3		0.46		0.82	

In contrast, A_2-subtype granitoids are considered to be derived from the subcontinental lithosphere or lower crust. They show a geochemical signature strongly different from OIB, and are frequently emplaced in post-collisional, that is post-orogenic settings. The emplacement of these granitoids usually follows after the end of compressional tectonics (10–20 Ma after). The A_2-subtype is the most common A-type granitoid formed during rifting caused by extension and thinning of continental crust (as a result of post-subductional and post-collisional processes). Rifting is accompanied by the ascent and emplacement of hot mantle magmas, which bear traces of the interaction with crustal magmas (Grebennikov 2014).

High Ce/Nb and Y/Nb ratios indicate that the Požega granite can be assigned to the A_2-subgroup (Fig. 11). Y/Nb ratios >1.2 (Požega granite: 1.7–2.6) suggest that corresponding magmas

might have received contributions from the upper continental crust (UCC). The relatively high Zr saturation temperatures reaching 950 °C, are also typical for A-type granites (e.g., Eby 2011).

Potential magma source

The origin of A-type granites is a long-standing geological problem and several petrogenetic interpretations have been proposed: (1) direct fractionation of mantle-derived magma (e.g., Turner et al. 1992), (2) mixing between mantle and crustal melts (e.g., Mingram et al. 2000), and (3) partial melting of the lower crust (e.g., Clemens et al. 1986; Frost et al. 1999). Interpretations (1) and (2) are not likely to be related to the Požega A_2-subtype of granite for the following reasons: (1) high concentrations of Ce, corresponding to values of the UCC (Table 2), and HFSE (particularly high Zr contents) are not consistent with a mafic/mantle precursor, which should be characterized by low abundances of these elements; (2) the Požega granite is devoid of phenocrysts, xenocrysts, wall-rock and mafic xenoliths, as well as inherited zircon, which can be interpreted as field and mineralogical evidence for the absence of magma mixing. Occurrence of zoned feldspar grains with an inner zone showing twin lamellae (almost always at least slightly sericitized) overgrown by a perthitic outer zone devoid of alterations could have resulted from a mixing event or at least an additional input of a slightly chemically different magma. Thus, magma mixing cannot be totally excluded. Nevertheless, the balance of evidence for the Požega granite favours the interpretation that the A_2-subtype granite magma was likely generated by partial melting of the lower crust (e.g., Eby 1992; Frost et al. 1999; Bonin 2007). The Zr/Hf ratio (34–42) of the Požega granite falls in the range for the average crust and, thus, supports this interpretation. The low Rb/Sr ratios (0.5–1.8) are consistent with the derivation of this magma from the lower crust although interaction with mantle-derived melts cannot be excluded. The boundary between the continental crust and the subcontinental lithospheric mantle is characterized by vertical and horizontal heterogeneities due to lower crust–mantle interactions (Kempton et al. 1990; Burov et al. 2007). Generally, two crustal sources are considered for A-type granites: (1) an anhydrous lower crustal granulite residue from which granitic melts had been previously extracted (Collins et al. 1982; Zhao et al. 2008) and (2) granodioritic to tonalitic rocks (Skjerlie & Johnston 1993; Patiño Douce 1997). The former crustal source (1) is depleted in K_2O and SiO_2 and enriched in CaO and Al_2O_3, which (except for Al_2O_3) is not compatible with the chemistry of the Požega granite. The latter crustal source (2) would produce strongly peraluminous melts by a low degree of partial melting of magnesian tonalite at 10 kbar (Skjerlie & Johnston 1993), whereas this process at 4 kbar (950 °C) induces metaluminous melts (Patiño Douce 1997). Patiño Douce (1997) and Frost & Frost (2011) suggest that partial melting of tonalitic to granodioritic crust produces alkali-calcic to calc–alkalic granitoid melts that are metaluminous at low pressures and peraluminous at high pressures. Since the Požega granite is peraluminous, tonalite from the lower crust is a potential candidate for the source rock of the A-type magma. High mafic index numbers ($FeO_T/FeO_T+MgO=0.97–0.98$) and

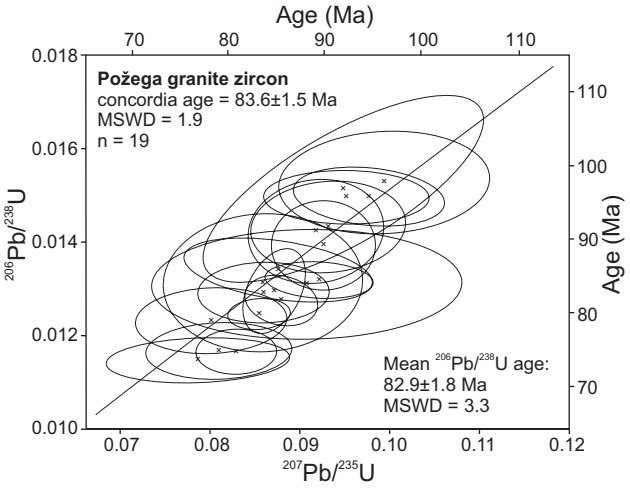

Fig. 9. U–Pb concordia diagram for zircon from the Požega granite (sample GV1). Error ellipses relate to 2 sigma errors. Weighted average ages, 2 sigma errors and MSWD are given in Table 5.

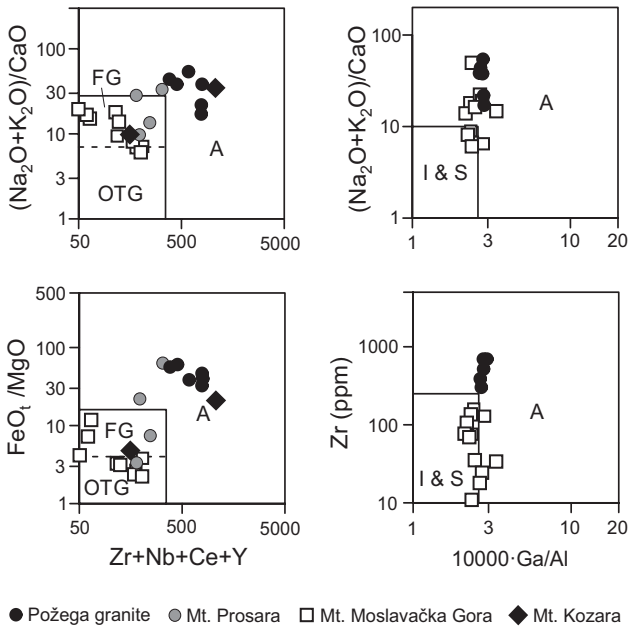

Fig. 10. Discrimination diagrams for granites after Whalen et al. (1987). I, S, and A denote I-, S-, and A-type granites, respectively. FG — fractionated felsic granites; OTG — unfractionated M-, I-, and S-type granites. Geochemical data for the Mt. Moslavačka Gora are from Starijaš et al. (2010), Balen & Broska (2011), and Balen & Petrinec (2011), for the northern part of Mt. Kozara are from Ustaszewski et al. (2009) and Cvetković et al. (2014), and for the Mt. Prosara are from Pamić & Injuk (1988) and Ustaszewski et al. (2009).

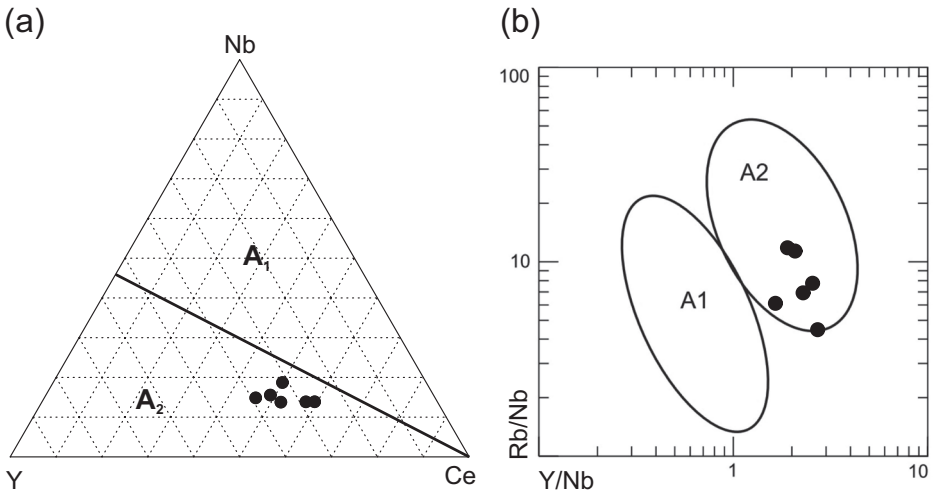

Fig. 11. Data for Požega granite samples plotted on discrimination diagrams for A-type granites after Eby (1990, 1992). A_1 and A_2 are subtypes.

low MgO contents (0.04–0.11 wt. %) in the Požega granite are similar to those of magmas that have been argued to be derived from mafic lower crust (Frost & Frost 1997; Frost et al. 1999).

Additionally, the REE patterns of the Požega granite do not show the tetrad-effect (McLennan 1994) implying absence of a significant fluid content in the melt. The element distribution is CHARAC (CHArge and RAdius Controlled; Bau 1996), according to the determined Zr/Hf (34–42) and Y/Ho (26–31) ratios in the Požega granite. The former ratio also suggests a crustal contribution. However, relatively low Rb/Sr ratios (0.5–1.8) imply (see above) that a portion of the magma may have originated in the mantle and/or deeper crustal levels at depths >20 km (Condie 1973). The K/Rb ratio (212–288) is also consistent with an input of material from the lower crust (Taylor 1965; Shaw 1968) which fits well with the K/Ba (53–79) and Ba/Rb (2.9–5.4) ratios (Mason 1966). Therefore, the Požega granite magma can be most likely derived from partial melting (and mixing) of a lower crustal and/or a subduction-derived mafic component at pressures around 10 kbar.

Implications of zircon geochemistry and inclusions for magma emplacement

As outlined in the section "Zircon – External morphology and internal structure", zircon crystals in the Požega granite sample GV1 show the morphological characteristics expected for lower crust/upper mantle magma where zircon crystallized at a relatively high and constant temperature. The positive Ce anomaly in the zircon REE patterns (Fig. 8) provides evidence for a positive oxidation potential of the magma. Geochemical trends such as those shown in Fig. 8a and b are expected for unaltered zircon of magmatic origin formed by melting of crustal material (Hoskin & Ireland 2000). The Zr/Hf ratio of zircon is higher than that of the whole rock (55 vs. 39). Using the scheme proposed by Pupin (2000), Zr/Hf ratios of zircon (41–69, mean 55) point to mantle-derived alkali granitic melt. Zircon crystallizing from a water-unsaturated melt is Hf-depleted (Erdmann et al. 2013), which means that the Zr/Hf ratios of the zircon should be higher compared to this ratio in the whole-rock. This is corroborated by the zircon morphology typical for tholeiitic and alkali-granitic series, but also common for A-type granites (Whalen et al. 1987) characterized by high temperature crystallization and lack of water (dry system).

The minerals kumdykolite and kokchetavite were found as tiny inclusions (<10 μm) in zircon. Although such minerals were originally considered to be indicators of ultrahigh pressure (Hwang et al. 2004, 2009; Németh et al. 2013; Kotková et al. 2014), Ferrero et al. (2016) and Ferrero & Angel (2018) showed that these minerals represent metastable phases in melt inclusions and as such point to rapid crystallization. Thus, cooling must have been fast, which is further supported by the occurrence of hematite with crystallographically oriented ilmenite exsolutions (Fig. 3b), perthite (Fig. 3d), and zircon aspect ratios between 1.7:1 and 2.9:1.

Constraints from thermometry

The zircon saturation temperature can be used to estimate the minimum melting temperature for a granite lacking inherited zircon (Miller et al. 2003). The T_{Zr} calculation using the equation by Watson & Harrison (1983) indicates that Zr became saturated in the magma of the Požega granite between 860 and 950 °C (Fig. 12). Using the newer and improved model for aluminous and alkaline melts after Gervasoni et al. (2016), almost identical temperatures were obtained (830–950 °C). To reach the average calculated

temperature of ca. 900 °C complete zircon dissolution is required. Due to the lack of appropriate minerals for barometric constraints, a quantitative pressure evaluation for the Požega granite is not possible.

If we combine the calculated temperature range with the depth of magma generation in the upper mantle and/or deeper crustal levels around 30 km (8–10 kbar), the geothermal gradient obtained is 30 °C/km. This is well within the range of 20–50 °C/km defined by Thompson & Connolly (1995) and Thompson et al. (2001) for back-arc settings.

Geodynamic context of the occurrence of the A-type granite at Mt. Požeška Gora

Discrimination diagrams of Pearce et al. (1984) (Fig. 13) place the Požega granite in a within-plate setting or, less clearly, in a volcanic arc setting. Furthermore, Pearce's (1996) diagrams define it as a post-collision granite. These discrimination diagrams also show that the Požega granite plots differently compared to contemporaneous granites or acidic intrusive rocks from the western part of the Sava Zone at Mt. Moslavačka Gora (82±1 Ma; Starijaš et al. 2010; Balen & Broska 2011; Balen & Petrinec 2011), in the northern part of Mt. Kozara (81.60±0.12 Ma age here is for effusive rock

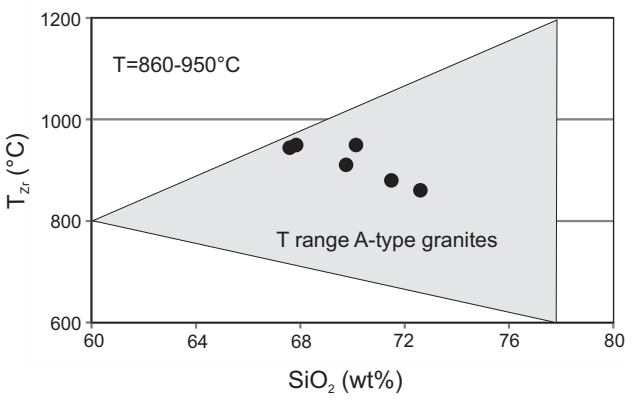

Fig. 12. Diagram of zircon saturation temperatures (T_{Zr}; Watson & Harisson 1983) vs. SiO_2 for the Požega granite. Shaded area after Eby (2011) shows range of temperatures typical for A-type granites.

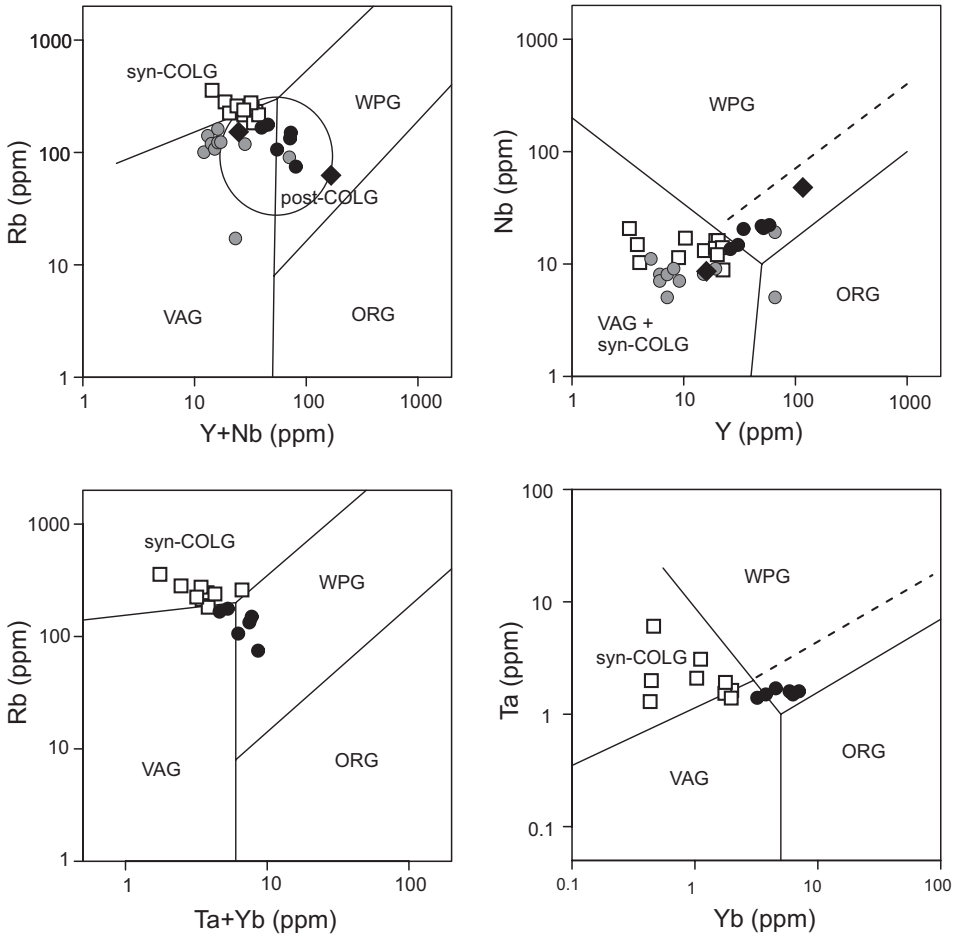

Fig. 13. Geotectonic discrimination diagrams for granites after Pearce et al. (1984) and Pearce (1996). References for geochemical data and symbols are the same as for Fig. 10. VAG — volcanic arc granites, WPG — within-plate granites, syn-COLG — syn-collision granites, ORG — ocean-ridge granites, post-COLG — post-collision granites.

(rhyolite); Ustaszewski et al. 2009; Cvetković et al. 2014) and at Mt. Prosara (82.68±0.13 Ma; Pamić & Injuk 1988; Pamić & Lanphere 1991; Ustaszewski et al. 2009) implying a different evolution (Fig. 13). Whereas Mt. Prosara leucogranite samples are comparable to those from the Požega granite, the Mt. Moslavačka Gora (S-type syn-collision granite) and N Kozara (oceanic plagiogranite, quartz diorite) samples are less similar. Although some of the N Kozara rhyolites (Cvetković et al. 2014) show a pronounced A-type signature, the possible genetic connection to the Slavonia area granite and rhyolites (Mt. Požeška Gora, Pamić et al. 1988/1989; Mt. Papuk, Balen & Petrinec 2014) remains to be resolved.

We relate the origin of the Požega granite to the collisional environment between the Adria and Tisia microplates where a subducted plate (Adria) probably caused the mantle to rise during the Mesozoic, leading to extensional rift processes in the suture zone. A provisional scenario for the origin of the Požega granite is outlined in Fig. 14. This granite with its specific zircon typology provides geochemical and mineralogical evidence that the corresponding magma of the A_2-type originated at great depths and at high temperatures at lower crustal/mantle levels and intruded (according to inclusions in zircon) rapidly upper crustal levels. The granite crystallization and following geological processes like exhumation and erosion were also fast, taking into account exsolution and micrographic textures and a narrow time span between the here obtained Santonian zircon age and the occurrence of corresponding granite pebbles and fragments at the base of the Santonian–Campanian–Maastrichtian stratigraphic column (e.g., Jamičić 2007).

The subsequent crustal extension caused rhyolitic volcanism and younger extension-related basaltic volcanism along deep faults (Belak et al. 1998). The zircon age of 83.6±1.5 Ma obtained in our study indicates that the transition from compression to extension of the Sava Zone began at least in the Late Cretaceous. These data contradict the previously reported Maastrichtian age (71.5±2.8 Ma, Rb/Sr isochron) for three granite and two apparently cogenetic rhyolite samples (Pamić et al. 1988), but are consistent with the stratigraphic constrains (Šparica et al. 1979, 1980; Jamičić 2007).

Conclusions

The geochemistry and petrology of the Požega granite, and particularly the zircon typology and chemistry, indicate that melting of lower continental crust composed of heterogeneous material was triggered by the heat from the upper mantle below the Sava Zone. The subsequent ascent of this granitic magma was focused along the Sava Zone segment of the Cretaceous collisional zone between Europe and Adria and was controlled by the subduction of the Adria lithosphere. The hot and dry granitic magma was emplaced at upper crustal levels after rapid ascent that had started from depths of about 30 km at temperatures of ca. 900 °C.

The A-type Požega granite was generated in an extensional tectonic environment (rift zone, back-arc setting?) located at the suture zone where subduction of the Adria plate underneath the European plate took place. The occurrence of this A-type granite indicates the beginning of the tectonic transition from compression to extension at 83.6±1.5 Ma to form a minor extensional basin.

Acknowledgements: The authors are grateful to Thomas Theye for help during microprobe work. Many thanks are also due to Dirk Spengler for discussions and graphical help. Our gratitude goes to Mirko Belak, Vladica Cvetković and Geologica Carpathica editor for constructive comments. This work was supported by the Croatian Science Foundation, project IP-2014-09-9541. Analytical works performed in Banská Bystrica were co-financed by ERDF through the projects ITMS: 26220120064, ITMS: 26250120034 and Slovak Research and Development Agency APVV-15-0050. DB and PS would like to thank the University of Zagreb Commission for the Rector's Award.

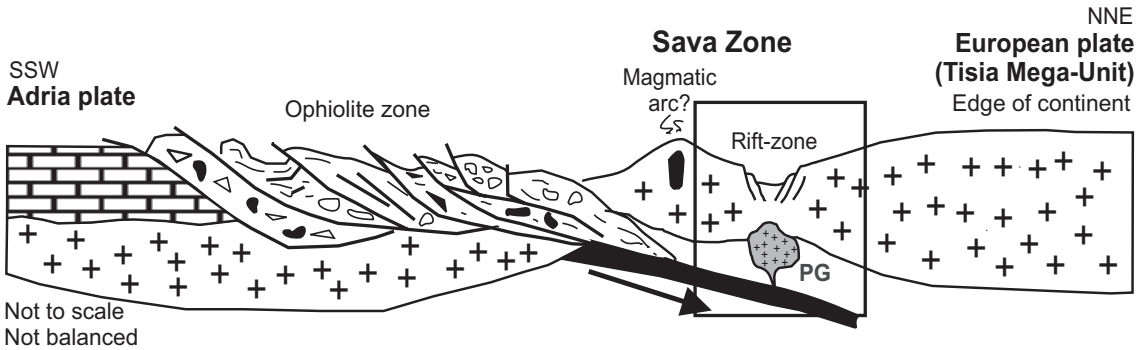

Fig. 14. Schematic cross-section through the suture zone between the Adria and Tisia microplates showing a plausible scenario for the Alpine geodynamic evolution of the northern edge of the Adria plate boundary. Approximate position of the Požega granite is marked with a rectangle. The model is slightly modified after Pamić et al. (2002a, b).

References

Balen D. & Broska I. 2011: Tourmaline nodules – products of devolatilization within the final evolutionary stage of granitic melt? In: Sial A.N., Bettancourt J.S., De Campos C.P. & Ferreira V.P. (Eds.): Granite-Related Ore Deposits. *Geol. Soc. Spec. Publ.* 350, 53−68. https://doi.org/10.1144/SP350.4

Balen D. & Petrinec Z. 2011: Contrasting tourmaline types from peraluminous granites: a case study from Moslavačka Gora (Croatia). *Mineral. Petrol.* 102, 117−134. https://doi.org/10.1007/s00710-011-0164-8

Balen D. & Petrinec Z. 2014: Development of columnar jointing in albite rhyolite in a rapidly cooling volcanic environment (Rupnica, Papuk Geopark, Croatia). *Terra Nova* 26, 102–110. https://doi.org/10.1111/ter.12075

Bau M. 1996: Controls on the fractionation of isovalent trace elements in magmatic and aqueous systems: evidence from Y/Ho, Zr/Hf, and lanthanide tetrad effect. *Contrib. Mineral. Petrol.* 123, 323–333. https://doi.org/10.1007/s004100050159

Belak M., Halamić J., Marchig V. & Tibljaš D. 1998: Upper Cretaceous–Paleogene tholeiitic basalts of the southern margin of the Pannonian Basin: Požeška gora Mt. (Croatia). *Geologica Croatica* 51, 2, 163–174. https://doi.org/10.4154/GC.1998.13

Belousova E.A., Walters S., Griffin W.L., O'Reilly S.Y. & Fisher N.I. 2002: Igneous zircon: trace element composition as an indicator of source rock type. *Contrib. Mineral. Petrol*. 143, 602–622. https://doi.org/10.1007/s00410-002-0364-7

Bonin B. 2007: A-type granites and related rocks: evolution of a concept, problems and prospects. *Lithos* 97, 1–29. https://doi.org/10.1016/j.lithos.2006.12.007

Boynton W.V. 1984: Geochemistry of the rare earth elements: meteorite studies. In: Henderson P. (Ed.): Rare earth element geochemistry. *Elsevier*, 63–114.

Burov E., Guillou-Frottier L., d'Acremont E., Le Pourhiet L. & Cloetingh S. 2007: Plume head–lithosphere interactions near intra-continental plate boundaries. *Tectonophysics* 434, 15–38. https://doi.org/10.1016/j.tecto.2007.01.002

Clemens J.D., Holloway J.R. & White A.J.R. 1986: Origin of an A-type granite: experimental constraints. *Am. Mineral*. 71, 317−324.

Collins W.J., Beams S.D., White A.J.R. & Chappell B.W. 1982: Nature and origin of A-type granites with particular reference to southeastern Australia. *Contrib. Mineral. Petrol*. 80, 189−200. https://doi.org/10.1007/BF00374895

Condie K.C. 1973: Archean magmatism and crustal thickening. *Geol. Soc. Am. Bull.* 84, 2981–2991.

Croatian Geological Survey 2009: Geological map of the Republic of Croatia, M 1:300,000 [Geološka karta Republike Hrvatske]. *Croatian Geological Survey, Department of Geology*, Zagreb (in Croatian).

Cvetković V., Šarić K., Grubić A., Cvijić R. & Milošević A. 2014: The Upper Cretaceous ophiolite of North Kozara – remnants of an anomalous mid-ocean ridge segment of the Neotethys? *Geol. Carpath.* 65, 117–130. https://doi.org/10.2478/geoca-2014-0008

Dachille F., Simons P.Y. & Roy R. 1968: Pressure–temperature studies of anatase, brookite, rutile and TiO_2-II. *Am. Mineral*. 53, 1929−1939.

De la Roche H., Leterrier J., Grandclaude P. & Marchal M. 1980: A classification of volcanic and plutonic rocks using R1R2-diagram and major element analyses – its relationships with current nomenclature. *Chem. Geol*. 29, 183–210. https://doi.org/10.1016/0009-2541(80)90020-0

Dickinson W. & Gehrels G. 2003: U–Pb ages of detrital zircons from Permian and Jurassic eolian sandstones of the Colorado Plateau, USA: paleogeographic implications. *Sediment. Geol.* 163, 29–66. https://doi.org/10.1016/S0037-0738(03)00158-1

Eby G.N. 1990: The A-type granitoids: a review of their occurrence and chemical characteristics and speculations on their petrogenesis. *Lithos* 26, 115–134. https://doi.org/10.1016/0024-4937(90)90043-Z

Eby G.N. 1992: Chemical subdivision of the A-type granitoids: petrogenetic and tectonic implications. *Geology* 20, 641–644.

Eby G.N. 2011: A-type granites: magma sources and their contribution to the growth of the continental crust. In: Seventh Hutton Symposium on Granites and Related Rocks, 50–51.

Erdmann S., Wodicka N., Jackson S.E. & Corrigan D. 2013: Zircon textures and composition refractory recorders of magmatic volatile evolution? *Contrib. Mineral. Petrol.* 165, 45–71. https://doi.org/10.1007/s00410-012-0791-z

Ferrero S. & Ross J.A. 2018: Micropetrology: Are Inclusions Grains of Truth? *J. Petrol.* 59, 1671–1700. https://doi.org/10.1093/petrology/egy075

Ferrero S., Ziemann M.A., Angel R.J., O´Brien P.J. & Wunder B. 2016: Kumdykolite, kokchetavite, and cristobalite crystallized in nanogranites from felsic granulites, Orlica–Snieznik Dome (Bohemian Massif): not evidence for ultrahigh–pressure conditions. *Contrib. Mineral. Petrol*. 171, 3. https://doi.org/10.1007/s00410-015-1220-x

Frezzotti M.L., Tecce F. & Casgali A. 2012: Raman spectroscopy for fluid inclusions analysis. *J. Geochem. Explor*. 112, 1–12. https://doi.org/10.1016/j.gexplo.2011.09.009

Frost C.D. & Frost B.R. 1997: Reduced rapakivi-type granites: the tholeiite connection. *Geology* 25, 647–650. https://doi.org/10.1130/0091-7613(1997)025<0647:RRTGTT>2.3.CO;2

Frost C.D. & Frost B.R. 2011: On ferroan (A-type) granitoids: their compositional variability and modes of origin. *J. Petrol*. 32, 39–53. https://doi.org/10.1093/petrology/egq070

Frost C.D., Frost B.R., Chamberlain K.R. & Edwards B.R. 1999: Petrogenesis of the 1.43 Ga Sherman batholith, SE Wyoming: a reduced rapakivi-type anorogenic granite. *J. Petrol.* 40, 1771–1802. https://doi.org/10.1093/petroj/40.12.1771

Frost B.R., Branes C.G., Collins W.J., Arculus R.J., Ellis D.J. & Frost C.D. 2001: A geochemical classification for granitic rocks. *J. Petrol.* 42, 2033–2048. https://doi.org/10.1093/petrology/42.11.2033

Fu Z., Liang Y., Wang S. & Zhong Z. 2013: Structural phase transition and mechanical properties of TiO_2 under high pressure. *Phys. Status Solidi B* 250, 2206–2214. https://doi.org/10.1002/pssb.201349186

Gervasoni F., Klemme S., Rocha-Júnior E.R.V. & Berndt J. 2016: Zircon saturation in silicate melts: a new and improved model for aluminous and alkaline melts. *Contrib. Mineral. Petrol.* 171, 21. https://doi.org/10.1007/s00410-016-1227-y

Grebennikov A.V. 2014: A-type granites and related rocks: petrogenesis and classification. *Russ. Geol. Geophys*. 55, 1074–1086. https://doi.org/10.1016/j.rgg.2014.10.011

Handy M.R., Ustaszewski K. & Kissling E. 2015: Reconstructing the Alps–Carpathians–Dinarides as a key to understanding switches in subduction polarity, slab gaps and surface motion. *Int. J. Earth Sci. (Geol. Rundsch.)* 104, 1–26. https://doi.org/10.1007/s00531-014-1060-3

Hoskin P.W.O. & Ireland T.R. 2000: Rare earth element chemistry of zircon and its use as a provenance indicator. *Geology* 28, 627–630. https://doi.org/10.1130/0091-7613(2000)28<627:REECOZ>2.0.CO;2

Hoskin P.W.O. & Schaltegger U. 2003: The composition of zircon and igneous and metamorphic petrogenesis. *Rev. Mineral. Geochem*. 53, 27–62. https://doi.org/10.2113/0530027

Hurai V., Huraiova M., Slobodnik M. & Thomas R. 2015: Geofluids – Developments in Microthermometry, Spectroscopy, Thermodynamics, and Stable Isotopes. *Elsevier*, 1–489.

Hwang S.L., Shen P., Chu H.T., Yui T.F., Liou J.G., Sobolev N.V., Zhang R.U., Shatsky V.S. & Zayachkovsky A.A. 2004:

Kokchetavite: a new potassium-feldspar polymorph from the Kokchetav ultrahigh-pressure terrain. *Contrib. Mineral. Petrol.* 148, 380–389. https://doi.org/10.1007/s00410-004-0610-2

Hwang S.L., Shen P., Chu H.T., Yui T.F., Liou J.G. & Sobolev N.V. 2009: Kumdykolite, an orthorhombic polymorph of albite, from the Kokchetav ultrahigh-pressure massif, Kazakhstan. *Eur. J. Mineral.* 21, 1325–1334. https://doi.org/10.1127/0935-1221/2009/0021-1970

Jamičić D. 2007: Upper Cretaceous deposits of the Požeška gora Mt. (Croatia). *Natura Croatica* 16, 105–120.

Janoušek V., Farrow C.M. & Erban V. 2006: Interpretation of whole-rock geochemical data in igneous geochemistry: introducing Geochemical Data Toolkit (GCDkit). *J. Petrol.* 47, 1255–1259. https://doi.org/10.1093/petrology/egl013

Kanzaki M., Xue X., Amalberti J. & Zhang Q. 2012: Raman and NMR spectroscopic characterization of high-pressure K-cymrite ($KAlSi_3O_8.H_2O$) and its anhydrous form (kokchetavite). *J. Mineral. Petrol. Sci*. 107, 114–119. https://doi.org/10.2465/jmps.111020i

Kempton P.D., Harmon R.S., Hawkesworth C.J. & Moorbath S. 1990: Petrology and geochemistry of lower crustal granulites from the Geronimo Volcanic Field, southeastern Arizona. *Geochim. Cosmochim. Acta* 54, 3401–3426. https://doi.org/10.1016/0016-7037(90)90294-U

King P.L., White A.J.R., Chappell B.W. & Allen C.M. 1997: Characterization and origin of aluminous a-type granites from the Lachlan Fold Belt, Southeastern Australia. *J. Petrol.* 38, 371–391. https://doi.org/10.1093/petroj/38.3.371

Kotková J., Škoda R. & Machovič V. 2014: Kumdykolite from the ultrahigh-pressure granulite of the Bohemian Massif. *Am. Mineral.* 99, 1798–1801. https://doi.org/10.2138/am.2014.4889

Ludwig K. 2003: User's Manual for Isoplot 3.00, A Geochronological Toolkit for Microsoft Excel. *Berkeley Geochron. Center Spec. Publ.* 4, Berkeley, 1–70.

Lužar-Oberiter B., Mikes T., Dunkl I., Babić Lj. & von Eynatten H. 2012: Provenance of Cretaceous synorogenic sediments from the NW Dinarides (Croatia). *Swiss J. Geosci.* 105, 377–399. https://doi.org/10.1007/s00015-012-0107-3

Martínez J.C., Massonne H.-J., Dristas J.A., Opitz J. & Angeletti M. 2020: Paleoproterozoic metamorphosed calc-alkaline dikes of the southwestern Río de la Plata craton, Tandilia belt of Argentina, record a prograde high-pressure, medium-temperature evolution. *J. South Am. Earth Sci.* 101, 102595. https://doi.org/10.1016/j.jsames.2020.102595

Mason B. 1966: Principals of Geochemistry, 3rd Edition. *John Wiley & Sons*, New York, 1–329.

Massonne H.-J., Opitz J., Theye T. & Nasir S. 2013: Evolution of a very deeply subducted metasediment from As Sifah, northeastern coast of Oman. *Lithos* 156–159, 171–185. https://doi.org/10.1016/j.lithos.2012.11.009

McLennan S.M. 1994: Rare earth element geochemistry and the "tetrad" effect. *Geochim. Cosmochim. Acta* 58, 2025–2033. https://doi.org/10.1016/0016-7037(94)90282-8

Miller C.F., McDowell S.M. & Mapes R.W. 2003: Hot and cold granites? Implications of zircon saturation temperatures and preservation of inheritance. *Geology* 31, 529–532. https://doi.org/10.1130/0091-7613(2003)031<0529:HACGIO>2.0.CO;2

Mingram B., Trumbull R.B., Littman S. & Gerstenberger H. 2000: A petrogenetic study of anorogenic felsic magmatism in the Cretaceous Paresis ring complex, Namibia: evidence for mixing of crust and mantle-derived components. *Lithos* 54, 1–22. https://doi.org/10.1016/S0024-4937(00)00033-5

Németh P., Lehner S.W., Petaev M.I. & Buseck P. 2013: Kumdykolite, a high-temperature feldspar from an enstatite chondrite. *Am. Mineral.* 98, 1070–1073.

Paces J.B. & Miller J.D. 1993: Precise U–Pb ages of Duluth Complex and related mafic intrusions, northeastern Minnesota: geochronological insights into physical, petrogenetic, paleomagnetic and tectonomagmatic processes associated with the 1.1 Ga midcontinent rift system. *J. Geophys. Res.* 98, 13997–14013. https://doi.org/10.1029/93JB01159

Pamić J. 1987: Young-Alpine alkali feldspar granites (alaskites) from Mt. Požeška Gora in Slavonia, northern Yugoslavia [Mladoalpinski alkalijsko-feldspatski graniti (aljaskiti) Požeške gore u Slavoniji]. *Geologija* 30, 183–205 (in Croatian).

Pamić J. 1993: Eoalpine to Neoalpine magmatic and metamorphic processes in the northwestern Vardar Zone, the easternmost Periadriatic Zone and the southwestern Pannonian Basin. *Tectonophysics* 109, 273–307. https://doi.org/10.1016/0040-1951(93)90135-7

Pamić J. 2002: The Sava-Vardar Zone of the Dinarides and Hellenides versus the Vardar Ocean. *Eclogae Geol. Helv.* 95, 99–113.

Pamić J. & Injuk J. 1988: Alpine granitoids from Mt. Prosara in northern Bosnia (Yugoslavia) [Alpinske granitoidne stijene planine Prosare u sjevernoj Bosni]. In: Zbornik referata naučnog skupa Minerali, stijene, izumrli i živi svijet BIH. Sarajevo, 93–103 (in Croatian).

Pamić J. & Lanphere M. 1991: A-type granites from the collisional area of the northernmost Dinarides and Pannonian Basin. *Neues Jahrb. Mineral. Abh.* 161, 215–236.

Pamić J., Lanphere M. & Mckee E. 1988: Radiometric ages of metamorphic and associated igneous rocks of the Slavonian Mountains in the southern part of the Pannonian basin. *Acta Geol*. 18, 13–39.

Pamić J., Injuk, J. & Jakšić M. 1988/1989: Some geochemical features of the Upper Cretaceous bimodal volcanic association from the Požeška Gore Mt. in Slavonija (northern Croatia, Yugoslavia) [Prilog geokemijskom poznavanju gornjokredne bimodalne vulkanske asocijacije Požeške gore u Slavoniji (Sjeverna Hrvatska, Jugoslavija)]. *Geologija* 31–32, 415–435 (in Croatian).

Pamić J., Belak M., Bullen T.D., Lanphere M.A. & McKee E.H. 2000: Geochemistry and geodynamics of a Late Cretaceous bimodal volcanic association from the southern part of the Pannonian Basin in Slavonija (northern Croatia). *Mineral. Petrol.* 68, 271–296. https://doi.org/10.1007/s007100050013

Pamić J., Tomljenović B. & Balen D. 2002a: Geodynamic and petrogenetic evolution of Alpine ophiolites from the central and NW Dinarides: an overview. *Lithos* 65, 113–142. https://doi.org/10.1016/S0024-4937(02)00162-7

Pamić J., Balen D. & Herak M. 2002b: Origin and geodynamic evolution of Late Paleogene magmatic associations along the Periadriatic-Sava-Vardar magmatic belt. *Geodin. Acta* 15, 209–231. https://doi.org/10.1016/S0985-3111(02)01089-6

Patiño Douce A.E. 1997: Generation of metaluminous A-type granites by low-pressure melting of calc-alkaline granitoids. *Geology* 25, 743–746. https://doi.org/10.1130/0091-7613(1997)025<0743:GOMATG>2.3.CO;2

Pearce J.A. 1996: Sources and settings of granitic rocks. *Episodes* 19, 120–125. https://doi.org/10.18814/epiiugs/1996/v19i4/005

Pearce J.A., Harris N.B.W. & Tindle A.G. 1984: Trace element discrimination diagrams for the tectonic interpretation of granitic rocks. *J. Petrol.* 25, 956–981.

Pupin J.P. 1980: Zircon and granite petrology. *Contrib. Mineral. Petrol*. 73, 207–220.

Pupin J.P. 2000: Granite genesis related to geodynamics from Hf-Y in zircon. *Trans. R. Soc. Edinburgh: Earth Sci.* 91, 245–256.

Pupin J.P. & Turco G. 1972: Une typologie originale du zircon accessoire. *Bull. Soc. Fr. Minéral. Cristallogr.* 95, 348–359.

Schmid S.M., Bernoulli D., Fügenschuh B., Matenco L., Schefer S., Schuster R., Tischler M & Ustaszewski K. 2008: The Alps–Carpathians–Dinarides connection: a compilation of tectonic units. *Swiss J. Geosci.* 101, 139–183. https://doi.org/10.1007/s00015-008-1247-3

Schmid S.M., Fügenschuh B., Kounov A., Matenco L., Nievergelt P., Oberhänsli R., Pleuger J., Schefer S., Schuster R., Tomljenović B., Ustaszewski K. & van Hinsbergen D.J.J. 2020: Tectonic units of the Alpine collision zone between Eastern Alps and western Turkey. *Gondwana Res.* 78, 308–374. https://doi.org/10.1016/j.gr.2019.07.005

Shaw D.M. 1968: A Review of K-Rb fractionation trends by covariance analyses. *Geochim. Cosmochim. Acta* 32, 573–601.

Skjerlie K.P. & Johanson A.D. 1993: Fluid-absent melting behavior of an F-rich tonalitic gneiss at mid-crustal pressures: implications for the generation of anorogenic granites. *J. Petrol.* 34, 785–815. https://doi.org/10.1093/petrology/34.4.785

Sláma J., Kosler J., Condon D.J., Crowley J.L., Gerdes A., Hanchar J.M., Horstwood M.S.A., Morris G.A., Nasdala L., Norberg N., Schaltegger U., Schoene N., Tubrett M.N. & Whitehouse M.J. 2008: Plesovice zircon – a new natural reference material for U–Pb and Hf isotopic microanalysis. *Chem. Geol.* 249, 1–35. https://doi.org/10.1016/j.chemgeo.2007.11.005

Shaulis B., Lapen T.J. & Toms A. 2010: Signal linearity of an extended range pulse counting detector: Applications to accurate and precise U-Pb dating of zircon by laser ablation quadrupole ICP-MS. Geochem. *Geophys. Geosyst*. 11, Q0AA11. https://doi.org/10.1029/2010GC003198

Starijaš B., Gerdes A., Balen D., Tibljaš D. & Finger F. 2010: The Moslavačka Gora crystalline massif in Croatia: A Cretaceous heat dome within remnant Ordovician granitoid crust. *Swiss J. Geosci.* 103, 61–82. https://doi.org/10.1007/s00015-010-0007-3

Streckeisen A. 1974: Classification and nomenclature of plutonic rocks. *Geol. Rundsch.* 63, 773–786.

Sun S.S. & McDonough W.F. 1989: Chemical and isotopic systematics of oceanic basalts: implications for mantle composition and processes. In: Saunders A.D. & Norry M.J. (Eds.): Magmatism in ocean basins. *Geol. Soc. Spec. Publ.* 42, 313–345.

Šparica M., Juriša M., Crnko J., Šimunić A., Jovanović Č. & Živanović D. 1979: Basic geological map of Yugoslavia in scale 1:100.000, sheet Nova Kapela L 33-108 [Osnovna geološka karta SFRJ M 1:100.000, list Nova Kapela L 33-108]. *Geološki Institut Zagreb, Federal Geological Institute Beograd* (in Croatian).

Šparica M., Juriša M., Crnko J., Šimunić A., Jovanović Č. & Živanović D. 1980: Basic geological map of Yugoslavia–explanatory notes for sheet Nova Kapela L33-108 [Tumač za list Nova Kapela L33-108]. *Geološki Institut Zagreb, Federal Geological Institute Beograd* (in Croatian).

Taylor S.R. 1965: The Application of Trace Element Data to Problems in Petrology. *Phys. Chem. Earth.* 6, 133–213.

Thompson A.B. & Connolly J.A. 1995: Melting of the continental crust: some thermal constraints on anatexis in continental collision zones and other tectonic settings. *J. Geophys. Res*. 100, 15565–15579. https://doi.org/10.1029/95JB00191

Thompson A.B., Schulmann K., Jezek J. & Tolar V. 2001: Thermally softened continental extensional zones (arc and rifts) as precursors to thickened orogenic belts. *Tectonophysics* 332, 115–141. https://doi.org/10.1016/S0040-1951(00)00252-3

Turner S.P., Foden J.D. & Morrison R.S. 1992: Derivation of some A-type magmas by fractionation of basaltic magma: an example from the Padthaway Ridge, South Australia. *Lithos* 28, 151–179. https://doi.org/10.1016/0024-4937(92)90029-X

Ustaszewski K., Schmid S.M., Lugović B., Schuster R., Schaltegger U., Bernoulli D., Hottinger L., Kounov A., Fügenschuh B. & Schefer S. 2009: Late Cretaceous intra-oceanic magmatism in the internal Dinarides (northern Bosnia and Herzegovina): implications for the collision of the Adriatic and European plates. *Lithos* 108, 106–125. https://doi.org/10.1016/j.lithos.2008.09.010

Ustaszewski K., Kounov A., Schmid S.M., Schaltegger U., Krenn E., Frank W. & Fügenschuh B. 2010: Evolution of the Adria–Europe plate boundary in the northern Dinarides: from continent–continent collision to back-arc extension. *Tectonics* 29, TC6017. https://doi.org/10.1029/2010TC002668

Vermeesch P. 2018: IsoplotR: a free and open toolbox for geochronology. *Geosci. Front.* 9, 1479–1493. https://doi.org/10.1016/j.gsf.2018.04.001

Wang X., Griffin W.L. & Chen J. 2010: Hf contents and Zr/Hf ratios in granitic zircons. *Geochem. J.* 44, 65–72.

Watson E.B. & Harisson T.M. 1983: Zircon saturation revisited: temperature and composition effects in a variety of crustal magma types. *Earth Planet. Sci. Lett.* 64, 295–304.

Whalen J.B., Currie K.L. & Chappell B.W. 1987: A-type granites: geochemical characteristics, discrimination and petrogenesis. *Contrib. Mineral. Petrol*. 95, 407–419. https://doi.org/10.1007/BF00402202

Whitney D.L. & Evans B.W. 2010: Abbreviations for names of rock-forming minerals. *Am. Mineral.* 95, 185–187. https://doi.org/10.2138/am.2010.3371

Zhao X.F., Zhou M.F., Li J.W. & Wu F.Y. 2008: Association of Neoproterozoic A- and I-type granites in South China: Implications for generation of A-type granites in a subduction-related environment. *Chem. Geol.* 257, 1–15. https://doi.org/10.1016/j.chemgeo.2008.07.018